nature communications

Article

https://doi.org/10.1038/s41467-025-57924-1

Astrocytic pleiotrophin deficiency in the prefrontal cortex contributes to stress-induced depressive-like responses in male mice

Received: 1 November 2024

Accepted: 3 March 2025

Published online: 14 March 2025

Check for updates

Dongmei Chi[1,2,4], Kun Zhang[1,4], Jianxing Zhang[1,4], Zhaoli He[1,4], Hongxia Zhou[1], Wan Huang[1], Yang Liu[2], Jingxiu Huang[1], Weian Zeng[1], Xiaohui Bai[3] ✉, Chaopeng Ou[1] ✉ & Handong Ouyang[1] ✉

Astrocytes are closely linked to depression, and the prefrontal cortex (PFC) is an important brain region involved in major depressive disorder (MDD). However, the underlying mechanism by which astrocytes within PFC contribute to MDD remains unclear. Using single-nucleus RNA sequencing analyses, we show a significant reduction in astrocytes and attenuated pleiotrophin-protein tyrosine phosphatase receptor type Z1 (PTN-PTPRZ1) signaling in astrocyte-to-excitatory neuron communication in the PFC of male MDD patients. We find reduced astrocytes and PTN in the dorsomedial PFC of male mice with depression induced by chronic restraint and social defeat stress. Knockdown of astrocytic PTN induces depression-related responses, which is reversed by exogenous PTN supplementation or overexpression of astrocytic PTN. The antidepressant effects exerted by astrocytic PTN require interaction with PTPRZ1 in excitatory neurons, and PTN-PTPRZ1 activates the AKT signaling pathway to regulate depression-related responses. Our findings indicate the PTN-PTPRZ1-AKT pathway may be a potential therapeutic target for MDD.

Major depressive disorder (MDD) is a prevalent mental disorder characterized by depressed mood, fatigue or loss of energy in daily life, anhedonia, and suicidal ideation[1]. MDD is a leading cause of disability worldwide, contributing significantly to the global burden of disease[2,3]. The increased incidence of suicide attempts and suicide-related death contributes to increased mortality in populations with MDD[4].

The pathogenesis of MDD is thought to be a result of the combined effects of genetic, environmental, psychological, and biological factors[1,5]. Multiple brain regions are involved in the pathology of MDD, including the prefrontal cortex (PFC), anterior cingulate cortex, hippocampus, amygdala, nucleus accumbens, and anterior insula[6–8]. The PFC is an important region related to MDD[9,10]. Positron emission tomography radioligand examination has revealed an increased distribution of enzymes regulating nonserotonergic monoamine metabolism within the PFC in patients with major depressive episodes[11]. Previous studies have shown structural and functional changes in the

[1]Department of Anesthesiology, State Key Laboratory of Oncology in South China, Guangdong Provincial Clinical Research Center for Cancer, Sun Yat-sen University Cancer Center, Guangzhou, P. R. China. [2]Department of Experimental Research, State Key Laboratory of Oncology in South China, Guangdong Provincial Clinical Research Center for Cancer, Guangdong Esophageal Cancer Institute, Sun Yat-sen University Cancer Center, Guangzhou, P. R. China. [3]Department of Anesthesiology, Guangdong Provincial Key Laboratory of Malignant Tumor Epigenetics and Gene Regulation; Sun Yat-sen Memorial Hospital, Sun Yat-sen University, Guangzhou, China. [4]These authors contributed equally: Dongmei Chi, Kun Zhang, Jianxing Zhang, Zhaoli He. ✉e-mail: baixhui@mail.sysu.edu.cn; oucp@sysucc.org.cn; ouyhd@sysucc.org.cn

dlPFC after treatment in MDD patients[12–14]. In clinical practice, treatment measures targeting the dlPFC lead to differences in the outcomes of the antidepressant effect and somatic symptoms in MDD patients[15,16]. The medial prefrontal cortex (mPFC) in rodents corresponds to the dorsolateral prefrontal cortex (dlPFC) in primates[17,18]. The role of the PFC in rodents in the pathogenesis of depression has also been widely studied[19–22]. However, the molecular etiology of MDD is complex and remains unclear.

Astrocytes, which are ubiquitously distributed across the brain and closely interact with neurons, play a crucial role in the maintenance of normal functions in the central nervous system[23]. The important role of astrocytes in the pathogenesis of MDD has been widely studied[24,25]. Astrocyte dysfunction in the mPFC contributes to aberrant functional connectivity in depression-related networks in mice[26]. Morphological changes in astrocytes are associated with MDD progression and the severity of depression-related behaviors[27–29]. Astrocyte pathology, including aberrant protein and mRNA expression of astrocyte markers such as glial fibrillary acidic protein (GFAP) and S100β, has been reported to be related to the development of MDD[30]. Over 25 years ago, researchers identified a significant reduction in the density and size of astrocytes within the dlPFC of depressed individuals[31]. Glial ablation in the PFC via toxins specifically targeting astrocytes efficiently induces depression-related behaviors in rats[32]. A reduction in the density of GFAP+ astrocytes in the hippocampus has also been observed in a mouse model of depression induced by chronic mild stress[33]. Depletion of PFC GFAP+ cells has been reported to induce anhedonia-like behavior but not anxiety-like deficits, which can be reversed by activating GFAP+ cells in the PFC[34]. However, how a reduction in the number of PFC astrocytes affects depression at the molecular level has not yet been fully elucidated.

MDD is a neurological disease characterized by synaptic dysfunction involving astrocytes, which are intimately involved in interactions with neuronal synapses and play a role in the processing of synaptic information[35]. Depression induced by chronic stress is closely associated with excitation-inhibition imbalances within brain regions[36]. Pleiotrophin (PTN), also known as heparin-binding growth-associated molecule, is a developmentally regulated and secreted growth factor. The PTN facilitates the maturation of newborn neurons[37], and depletion of the PTN may result in the loss of neurons[38]. Abnormalities in neurogenesis and neuronal functions is related to MDD[1,39], and astrocytes are involved in the modulation of neuronal activity, synaptic function and neuronal growth[30]. Previous studies have shown that transgenic mice with PTN overexpression have more astrocytes in the hippocampus, which suggests that the endogenous PTN level may be involved in the modulation of astrocytic responses[40,41]. In a study focused on cell-cell communication in traumatic brain injury, astrocytes were found to be the main source of upregulated PTN in the hippocampus during the subacute phase, and elevated PTN promoted neurite growth[42]. PTN derived from astrocyte have been reported to contribute to improving recovery from acute neuroinflammation[43]. However, whether the astrocytic PTN in the PFC participates in the pathogenesis of MDD via the modulation of neural growth or synaptic function remains unclear. A previous study revealed that a reduction in PTN induces learning and memory impairment in mice, and the underlying mechanism may involve interruption of the interaction between PTN and protein tyrosine phosphatase receptor type Z1 (PTPRZ1), a receptor of PTN, which further affects adult hippocampal neurogenesis by activating AKT signaling[44]. In a study of the hippocampus of insomnia-induced cognitively impaired mice, the expression of PTN was reduced, leading to reduced binding to PTPRZ1 on the postsynaptic membrane[45]. Abnormal regulation of PTN has been reported to be relevant to synaptic dysfunction[46,47]. The astrocytes and PTN in the dorsomedial PFC (dmPFC) may affect the development of MDD via the modulation of neurogenesis and synaptic function. However, whether astrocytic PTN regulates MDD by modulating the density size and morphology of astrocytes in the PFC remains unclear.

In this study, we observed that the astrocytic PTN in the dmPFC was decreased in a stress-induced mouse model of depression. PTN activity in astrocytes in the dmPFC was sufficient to alleviate depression-related behaviors, increase neuronal excitability, and enhance synaptic signaling transmission. The effects of the astrocytic PTN in the dmPFC on depression required interaction with PTPRZ1 in excitatory neurons, which further affected phosphorylated AKT signaling. In conclusion, our findings reveal that the interaction of the astrocytic PTN in the PFC with PTPRZ1 in excitatory neurons is a potential target for MDD treatment.

Results

A single-nucleus transcriptomic atlas of the human prefrontal cortex in major depressive disorder patients and psychiatrically healthy controls

Many studies have indicated a critical role of the prefrontal cortex in the pathophysiology of major depressive disorder[34]. To elucidate the cellular composition and potential mechanisms of MDD in this region, we reanalyzed snRNA-seq data from Brodmann area 9 (BA9) in the dlPFC of 17 male patients who died during an episode of MDD and the other 17 from matched mentally healthy male individuals (GSE144136, Supplementary Fig. 1A, Supplementary Data 1). After quality control filters (see "Methods"), a total of 71,565 nuclear transcriptomes from the 34 brains were retained for subsequent analysis, of which 39,801 nuclei originated from MDD patients and 31,764 nuclei from controls (Fig. 1A, B, Supplementary Fig. 1B, and Supplementary Data 2). We conducted snRNA-seq data analysis following the Seurat pipeline and integrated this dataset on the basis of individual samples using the Harmony algorithm to correct for the batch effect (see Methods). The uniform mixing of samples and groups suggested effective correction of the batch effect. The nuclei were classified into seven major cell types (Fig. 1A, C, Supplementary Fig. 1C, and Supplementary Data 3) on the basis of canonical marker expression, including excitatory neurons ($n = 46{,}180$), identified by the expression of SATB2, SLC17A7, and CAMK2A; inhibitory neurons ($n = 13{,}641$), marked by GAD1 and GAD2; astrocytes (Astro, $n = 3510$), which were positive for GFAP; oligodendrocytes (Oligo, $n = 4662$), marked by MBP; oligodendrocyte precursor cells (OPC, $n = 2139$), which were positive for PCDH15; endothelial cells (Endo, $n = 330$), which expressed CLDN5 and VTN; and microglia/macrophage (Micro/Macro, $n = 1103$), defined by their classical markers CX3CR1 and MRC1. Given the high-resolution advantage of single-nucleus data, we further annotated the excitatory or inhibitory neuronal populations into more refined subtypes on the basis of distinct gene expression patterns, allowing for a more detailed characterization of cortical cellular architecture (see "Methods" for a full list of markers for neuron subclusters; Fig. 1D, E and Supplementary Data 3). Overall, our clustering results were consistent with those of previous studies of snRNA-seq analysis of the human prefrontal cortex[48].

Astrocyte subsets may be key regulators of the pathophysiology of MDD

The degree of infiltration of each cell type may reflect their distinct functional roles. To assess these differences, we utilized multiple methods to compare the changes in cell proportions between the two groups. Ro/e analysis revealed a significant decrease in the proportions of astrocytes, endothelial cells, OPCs, and oligodendrocytes in the MDD group, whereas the proportions of neurons and Micro/Macros were modestly increased. Notably, the number of astrocytes exhibited the greatest reduction (Fig. 1F). The results of the Wilcoxon test with the Benjamini–Hochberg procedure between groups further confirmed the significant reduction in the proportion of astrocytes in MDD patients (Astro, $P_{adj} = 0.0045$; Endo, $P_{adj} = 0.041$; Excit_neuron,

https://doi.org/10.1038/s41467-025-57924-1

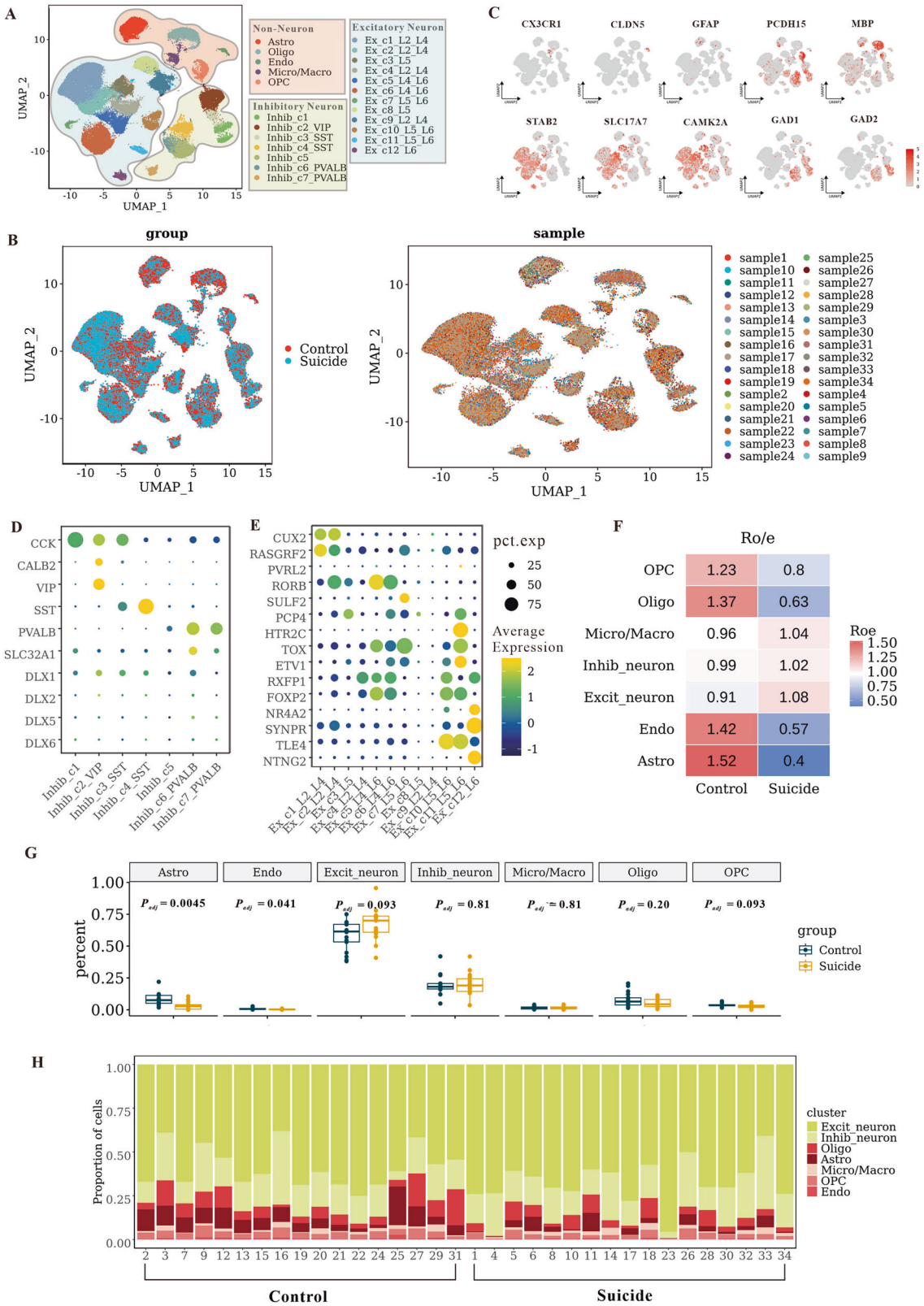

$P_{adj} = 0.093$; Inhib_neuron, $P_{adj} = 0.81$; Micro/Macro, $P_{adj} = 0.81$; Olig, $P_{adj} = 0.20$; OPC, $P_{adj} = 0.093$; Fig. 1G, Supplementary Data 4 and 5). In addition, the cell composition of each sample demonstrated a consistent decrease in astrocytes across all MDD samples compared with controls, eliminating the influence of outliers (Fig. 1H).

MDD is a disease closely related to genetic background[1]. To investigate how these genetic variants in relevant cell types mediate the disease at the single-cell level, we performed an integrated analysis of GWAS data and single-cell data using scPagwas algorithm (see "Methods", Supplementary Data 5). We found that astrocytes with higher trait-relevant scores (TRSs) showed the strongest enrichment in MDD patients (Supplementary Fig. 2A). Consistently, astrocytes were significantly associated with MDD at the cell type level (astro $P_{adj} = 1.11 \times 10^{-11}$; Supplementary Fig. 2B, and Supplementary Data 5).

Fig. 1 | Single-nucleus atlas of the human prefrontal cortex in major depressive disorder patients and psychiatrically healthy controls. A UMAP plots of 71,565 single nuclei grouped into nonneurons, including astrocytes, oligodendrocytes, oligodendrocyte precursor cells, endothelial cells, microglia/macrophages, excitatory neurons and inhibitory neurons. Each dot represents a single nucleus and is colored according to the cell type. Astro astrocytes, Oligo oligodendrocytes, OPC oligodendrocyte precursor cells, Endo endothelial cells, Micro/Macro microglia/macrophage, Ex excitatory neurons, Inhib inhibitory neurons, L layer (i.e., Ex_c1_L2_L4, excitatory neurons of the c1 subtype from cortex layer 2 to layer 4). **B** UMAP plot of the above single cells colored according to their group (left panel) or sample origin (right panel). **C** Feature plots showing the normalized expression of marker genes for each cell type. Each dot represents a single cell, and the depth of color from gray to red represents low to high expression. **D**, **E** Dot plot showing the normalized expression of marker genes for each subtype of inhibitory (**D**) or excitatory neurons (**E**). The depth of color from blue to yellow represents low to high expression, and the size of the circles represents the proportion of expression, increasing from small to large. **F** Group prevalence of cell clusters estimated by the Ro/e score (34 snRNA-seq) (see "Methods"). **G** Box plots showing the proportions of cell clusters in the suicide and control groups ($n = 34$). The centerlines denote median values, and the whiskers denote 1.5× the interquartile range. *P* values were calculated using two-sided Wilcoxon tests and adjusted for multiple comparisons via the Benjamini–Hochberg correction method. **H** Bar plots showing the proportion of each cell type in suicide or control patients. Each bar represents an individual patient, with cell proportions coded as different colors for cell types on the right. See Supplementary Data 5 for statistical details, including the statistical test used for data analysis and the exact *P* value. Source data are provided as a Source Data file.

Taken together, astrocytes not only showed the most significant change in cell proportions but were also identified as the key cell type by which genetic variants influence MDD, supporting their critical role in the pathophysiology of MDD.

Astrocytes markedly influence excitatory neurons in MDD, and their interaction via PTN pathway signaling is significantly reduced

To explore intercellular communication and discover major signaling changes in response to disease, we performed CellChat analysis (Supplementary Fig. 2A). We found that in both the MDD and control groups, astrocytes, as sender cells, interact with mainly excitatory neurons, inhibitory neurons, OPCs, and oligodendrocytes in the human cortex (Fig. 2A). The largest communication change was observed between astrocytes and excitatory neurons (Fig. 2B). Furthermore, by comparing the overall probability of communication between astrocytes and excitatory neurons in the cortex of the MDD and control groups, we found that five pathways were observed to be active in MDD, including the NCAM, NEGR, EPHA, NGL, and SEMA3 (Fig. 2C and Supplementary Fig. 3C) pathways. Among these pathways, 16 out of 29 signaling pathways showed decreased activity, including seven classic pathways related to neurotrophic support and neuromodulation, such as the PTN, PSAP, and SEMA series (Fig. 2C, Supplementary Fig. 3C, E–H).

Astrocytic PTN in the hippocampus has been reported to be related to the regulation of neurogenesis in traumatic brain injury[42], and aberrant PTN expression may impair synaptic function[46]. In the depression model, we investigated the interaction between astrocytic PTN and molecules in excitatory neurons. Specific to the PTN signaling pathway, CellChat revealed that its related ligand–receptor pairs, PTN–PTPRZ1, PTN–SDC3, PTN–NCL, and PTN–ALK, were also significantly decreased in the communication from Astro to Ex_L2–L6 (Fig. 2E and Supplementary Fig. 3D), corresponding to the PTN overall pathway change (Fig. 2D). Finally, the gene expression of key ligands in astrocytes and receptors in excitatory neurons related to the PTN signaling pathway was also significantly lower in the MDD group than in the control group, which is consistent with previous findings on pathways and ligand–receptor pairs (Astro PTN, $P_{adj} = 0.0043$; Excit–neuron PTPRZ1, $P_{adj} = 5.63 \times 10^{-23}$; SDC3, $P_{adj} = 1.18 \times 10^{-38}$; SDC4, $P_{adj} = 4.16 \times 10^{-18}$; NCL, $P_{adj} = 2.23 \times 10^{-32}$; ALK, $P_{adj} = 0.78$; Fig. 2F, Supplementary Fig. 1D, 4A, B, and Supplementary Data 5). In summary, CellChat analysis suggested that the decreased activity of the PTN signaling pathway in astrocyte-to-excitatory neuron communication may contribute to MDD pathogenesis.

The density of astrocytes and PTN expression in the dmPFC are decreased in a mouse model of depression

The above results suggest that the proportion of astrocytes and the expression of the astrocytic PTN in the human dlPFC are associated with the development of MDD. In terms of developmental origin, the human dlPFC corresponds to the dmPFC in rodents. To investigate the underlying mechanism of MDD, we prepared a wild-type (WT) C57BL/6 mouse model of depression under chronic restraint stress (CRS) (Fig. 3A) and chronic social defeat stress (Supplementary Fig. 7A), which successfully induced depression-related behaviors, including depressive-like behaviors in the FST, TST, SPT, and SIT, and anxiety-like behaviors in the OFT and EPM (Fig. 3B and Supplementary Fig. 7B). S100β, SOX9, and GFAP were chosen as markers for astrocytes. The WB and IHC results revealed that S100β, SOX9, and GFAP expression were lower in the mice subjected to CRS (Fig. 3C–H) or CSDS (Supplementary Fig. 7C–H) than in the control mice. These results suggest that the reduction in the number of astrocytes in the dmPFC is related to depression. To verify the CellChat analysis that astrocytic PTN may contribute to depression, additional in vivo experiments were performed. The mRNA (Fig. 3I) and protein expression (Fig. 3J) of PTN in the dmPFC were decreased in the CRS mice, in accordance with the IHC images (Fig. 3K). The costaining of S100β with PTN, SOX9, and PTN, GFAP, and PTN demonstrated that PTN was expressed in astrocytes in the dmPFC (Fig. 3L). To specifically validate the expression level of PTN in astrocytes, we isolated astrocytes from the dmPFC via an Anti-ASCA-2 MicroBeads Kit and subjected them to WB. Astrocytic PTN was significantly reduced in the CRS mice (Fig. 3M), similar to that in the CSDS mice (Supplementary Fig. 7I). Next, we explored neuronal excitability in the dmPFC. Both the amplitude and frequency of mEPSCs were significantly reduced in the depressed mice (Fig. 3N–P), indicating diminished presynaptic and postsynaptic transmission across synapses, which suggests attenuated synaptic plasticity. Moreover, the firing frequency was decreased in mice with depression (Fig. 3Q), demonstrating reduced neuronal excitability. The expression of postsynaptic density protein 95 (PSD95) was also reduced in CRS mice (Fig. 3R). The results of the sparse labeling test revealed that the density of dendritic spines was significantly lower in CRS mice than in control mice (Fig. 3S). These results demonstrate that the reduction of astrocytes and PTN expression in the dmPFC possibly contributes to the development of depression by reducing neuronal excitability and inducing synapse impairments.

Knockdown of PTN in the dmPFC promotes depression-related behaviors, reduces neuronal excitability, and leads to synapse impairments

Next, we bilaterally injected CMV-PTN-shRNA or CMV-PTN-shRNA NC into the dmPFC of WT mice to further investigate the effect of PTN on depression (Fig. 4A). The following experiments were performed three weeks after the application of the AAVs. The knockdown efficiency was verified through PCR, WB, and IHC analyses (Fig. 4B–D), which revealed that both the mRNA and protein expression of PTN in the dmPFC were significantly downregulated. In the behavioral tests, the mice exhibited much poorer performance in both depressive-like behaviors (FST, TST, SPT) and anxiety-like behaviors (OFT, EPM) after PTN was knocked down in the dmPFC (Fig. 4E), indicating that PTN in

https://doi.org/10.1038/s41467-025-57924-1

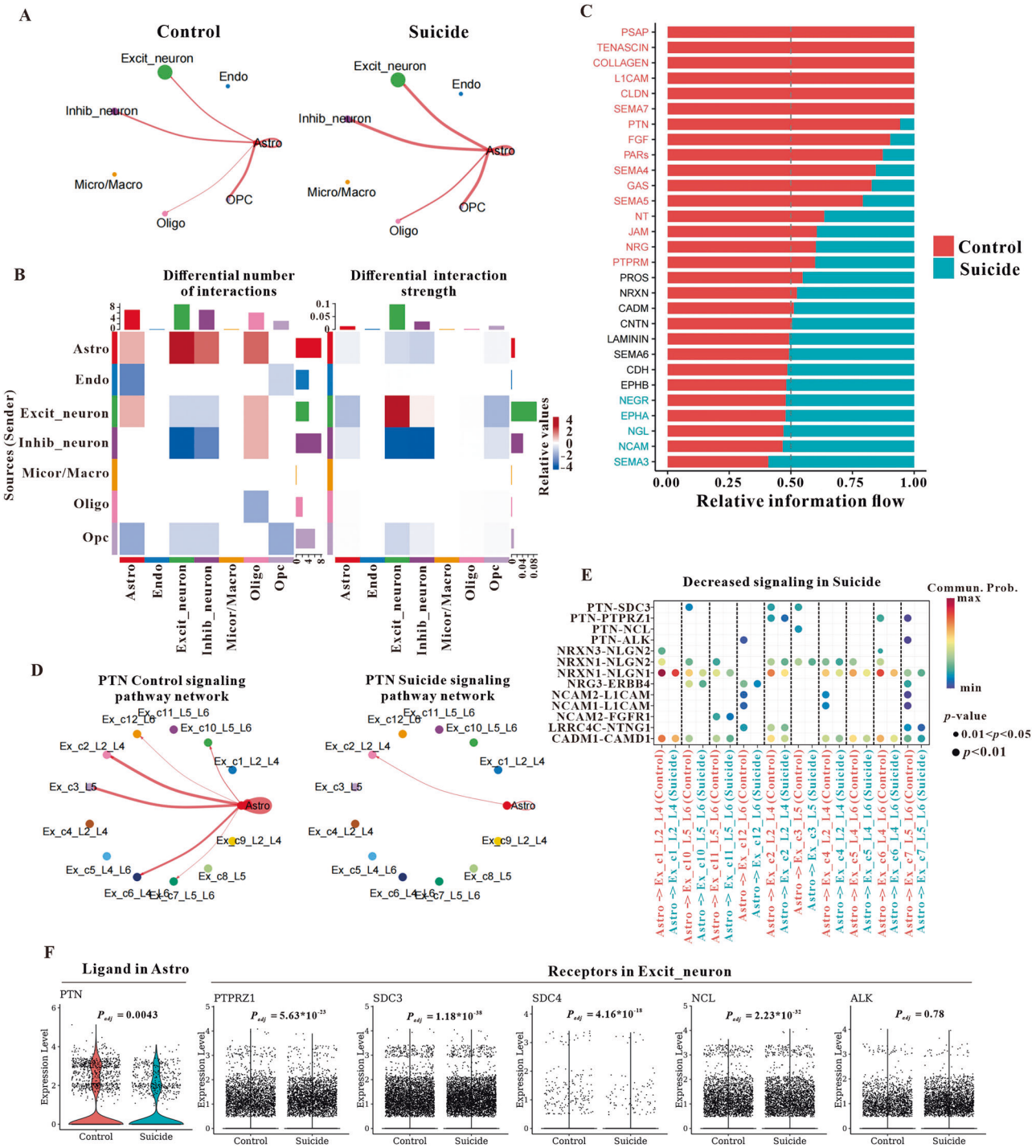

the dmPFC plays a crucial role in the modulation of depression-related behaviors. Using CMV-PTN-shRNA and CaMKIIα-EGFP labeling, the excitability of excitatory neurons in the dmPFC was tested in WT C57BL/6 mice. Both the amplitude and frequency of mEPSCs were reduced in the dmPFC PTN-knockdown mice (Fig. 4F–H), indicating that presynaptic and postsynaptic excitatory transmission were decreased when the dmPFC PTN was downregulated. In addition, knocking down dmPFC PTN expression significantly reduced the firing frequency (Fig. 4I). Given that the development of MDD is closely associated with neuronal synapses and synaptic information processing, we investigated how altered PTN expression affects neuronal synaptic morphology. As shown in Fig. 4J, a significant reduction in the density of dendritic spines was observed after the inhibition of PTN expression in the dmPFC. WB analysis revealed that PSD95 expression was attenuated after PTN was knocked down in the dmPFC of the mice (Fig. 4K). The results revealed that the knockdown of the PTN in the dmPFC led to synaptic impairments. Taken together, these findings suggest that PTN deficiency in the dmPFC facilitates depression, possibly through attenuated neuronal excitability and synaptic dysfunction.

Astrocytic-specific knockdown of the PTN in the dmPFC facilitates depressive-like responses

The results of the snRNA-seq analysis (Figs. 1 and 2) revealed that among the seven major cell types, astrocytes had the strongest association with MDD, and the PTN signaling pathway in

Fig. 2 | Cell–cell interaction network generated by CellChat showing that the PTN pathway is significantly decreased in the suicide group compared with the control group. A Circle plot showing the number of interactions between astrocytes (source) and various target cell populations in the two groups. **B** Heatmap showing the differential number of interactions or interaction strengths among different cell populations across the two groups. **C** Bar chart showing the comparison of the overall information flow of each signaling pathway or ligand–receptor pair between astrocytes and excitatory neurons between groups. Significant signaling pathways were ranked on the basis of differences in the overall information flow within the inferred networks between the two groups. Paired Wilcoxon tests were performed to assess the statistical significance. Pathways enriched in the control group are highlighted in red on the y-axis, whereas those enriched in the suicide group are in blue. **D** Circle plot showing the PTN signaling pathway from astrocytes (outgoing arrows) to all excitatory neuron subtypes (ingoing arrows) across the suicide and control groups. The circle sizes are proportional to the number of cells in each cell group, and the edge weights represent interaction strength. A thicker edge indicates a stronger signaling interaction. **E** Dot plot showing decreased ligand–receptor interactions between astrocytes and excitatory neuron subtypes in control (red) or suicide (blue) samples. Ligand–receptor interactions are indicated in columns. The means of the average expression levels of two interacting molecules are indicated by the color heatmap (bottom panel), with blue to red representing low to high expression. *P* values were obtained via one-sided permutation tests and are indicated by the circle size. **F** Violin plot showing the gene expression distributions of PTN signaling pathway-related key ligands in astrocytes and receptors in excit_neurons between the control (red) and suicide (blue) groups of astrocytes and excitatory neuron subtypes. *P* values were derived from two-sided Wilcoxon tests and adjusted for multiple comparisons via the Benjamini–Hochberg correction method. See Supplementary Data 5 for statistical details, including the statistical test used for data analysis and the exact *P* value. Source data are provided as a Source Data file.

astrocyte-to-excitatory neuron communication was linked to MDD pathogenesis. Co-stained imaging revealed that PTN is expressed in astrocytes in the dmPFC (Fig. 3L). To determine whether PTN derived from astrocytes affects MDD modulation, we utilized intraperitoneal injection of tamoxifen (TAM) and bilateral injection of DIO-PTN-shRNA into the dmPFC of Aldh1l1-Cre/ERT2 mice to specifically knock down astrocytic PTN (Fig. 5A). We separately examined the effects of tamoxifen on WT mouse behavior, and the results showed no significant changes (Supplementary Fig. 9C). To verify the knockdown efficiency of AAV transfection, astrocytes were isolated from dmPFC tissue of Aldh1l1-Cre/ERT2 mice and examined using PCR and WB, which revealed that both the mRNA and protein expression of PTN were reduced (Fig. 5B, C). In the behavioral studies, the astrocytic PTN-knockout Aldh1l1-Cre/ERT2 mice presented depression-related behaviors, including depressive-like behaviors and anxiety-like behaviors (Fig. 5D). After specifically knocking down the astrocytic PTN, both the amplitude and frequency of mEPSCs (Fig. 5E–G), as well as the firing frequency (Fig. 5H), were reduced in PTN-shRNA-treated mice. Moreover, downregulation of the astrocytic PTN also resulted in diminished dendritic spine density in dmPFC neurons (Fig. 5I) and decreased PSD95 expression (Fig. 5J). These findings suggest that the astrocyte-derived PTN in the dmPFC contributes to depression modulation by affecting neuronal excitability and synaptic functions.

Exogenous PTN supplementation or astrocytic PTN upregulation in the dmPFC exerts antidepressant effects

Since the depletion of astrocytic PTN in the dmPFC leads to depression-related behaviors, we investigated whether the exogenous administration of PTN into the dmPFC could elicit antidepressant-like effects. A cannula, positioned with its tip in the dmPFC of WT C57BL/6 mice for drug administration, was implanted prior to preparing the depression mouse model. The mice then received either PTN or control PBS injected into the dmPFC for further observation (Fig. 6A). The results showed that the infusion of exogenous PTN into the dmPFC effectively improved depression-related behaviors in stress-induced depressed mice (Fig. 6B). Similar experiments were conducted in depressed WT mice induced by CSDS, and similar results revealed that exogenous PTN supplementation also relieved the depression-related behaviors induced by CSDS (Supplementary Fig. 8A). With respect to neuronal excitability, exogenous PTN infusion significantly increased the amplitude and frequency of mEPSCs (Fig. 6C–E) and increased the firing frequency (Fig. 6F). In addition, increased dendritic spine density (Fig. 6G) and PSD95 expression levels (Fig. 6H) were detected following PTN infusion in the dmPFC of WT CRS mice.

In order to clarify the effects of endogenous PTN upregulation in the dmPFC on depression-related responses, we constructed AAV-DIO-PTN OE to overexpress astrocytic PTN in Aldh1l1-Cre/ERT2 mice (Fig. 6I). The efficiency of the constructed AAVs was verified by isolation of astrocytes and quantification of the astrocytic PTN through WB (Fig. 6J). As expected, overexpression of astrocytic PTN in the dmPFC of the Aldh1l1-Cre/ERT2 mice also sufficiently improved depression-related behaviors in both the CRS model (Fig. 6K) and the CSDS model (Supplementary Fig. 8B). Moreover, astrocytic PTN overexpression in the dmPFC of the Aldh1l1-Cre/ERT2 mice significantly increased the amplitude and frequency of mEPSCs (Fig. 6L–N), as well as the firing frequency in the CRS model mice (Fig. 6O). Greater dendritic spine density (Fig. 6P) and increased PSD95 expression (Fig. 6Q) were also observed following astrocytic PTN overexpression in the dmPFC in the CRS model mice. These findings reveal that increased astrocytic PTN expression in the dmPFC may alleviate depression-related responses.

Interaction between astrocytic PTN and excitatory-neuronal PTPRZ1 in the dmPFC mediates antidepressant effects

Next, we explored how the expression of astrocytic PTN affects other cells and affects depression-related responses. PTN exerts various effects by binding to several putative transmembrane receptors, such as PTPRZ1, ALK, and syndecan 3 (SDC3)[44]. Previous CellChat analysis (Fig. 2E) indicated that PTPRZ1, SDC3, SDC4, NCL, or ALK might interact with the PTN between astrocytes and excitatory neurons, contributing to MDD pathogenesis. Thus, we constructed corresponding AAVs to knock down PTPRZ1, SDC3, SDC4, NCL, or ALK in CaMKIIα+ excitatory neurons in the dmPFC of WT mice to evaluate their role in depression. The results revealed that the downregulation of SDC3, SDC4, NCL, or ALK in excitatory neurons did not elicit depression-related behaviors (Supplementary Fig. 6A–D). We then focused on the potential effects of PTPRZ1 on depression. According to previous studies, PTPRZ1 is most likely the membrane receptor through which PTN influences neural function[44,45]. Therefore, we investigated whether astrocytic PTN modulates antidepressant effects through its interaction with PTPRZ1 in excitatory neurons. We first examined the level of PTPRZ1 in WT mice and found that both the mRNA and protein expression of PTPRZ1 within the dmPFC were lower in CRS mice than in control mice (Fig. 7A–C). PTPRZ1 expression in isolated neurons was also significantly reduced in CRS mice (Fig. 7D) and CSDS mice (Supplementary Fig. 7J). We applied CaMKIIα-Cre and DIO-PTPRZ1-shRNA to the dmPFC to knock down the expression of PTPRZ1 in excitatory neurons in WT mice (Fig. 7E). To confirm the knockdown efficiency of AAV transfection, we utilized a neuron isolation MicroBeads kit to extract neurons from dmPFC tissue and confirmed that both the mRNA and protein expression of PTPRZ1 were significantly reduced (Fig. 7F, G). Behavioral tests revealed that downregulation of PTPRZ1 in excitatory neurons also induced depression-related behaviors, as the experimental mice exhibited worse performance in the OFT, EPM, FST, TST, and SPT (Fig. 7H). Knockdown of PTPRZ1 in excitatory neurons led to decreased neuronal excitability and synaptic impairment, as evidenced by the reduced amplitude and frequency of mEPSCs (Fig. 7I–K), lower firing frequency

https://doi.org/10.1038/s41467-025-57924-1

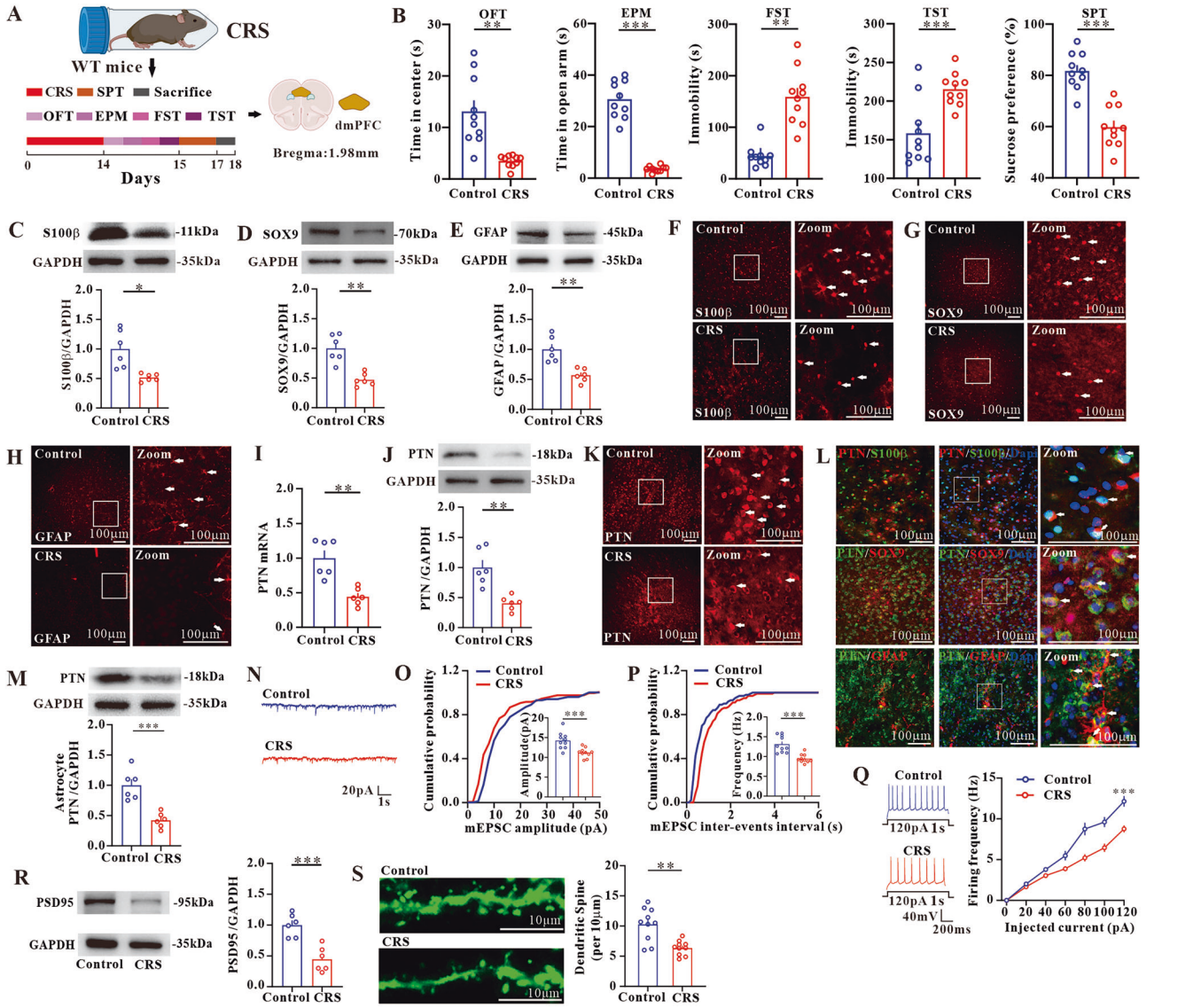

Fig. 3 | CRS leads to a decreased proportion of astrocytes and PTN expression in the dmPFC in mice. A Schematic of the experimental design (WT mice). **B** Analyses of behavioral tests, including the OFT, EPM, FST, TST, and SPT ($n = 10$ mice per group). **C**–**E** Quantification of S100β (**C**), SOX9 (**D**), and GFAP (**E**) expression by WB analyses ($n = 6$ mice per group). **F**–**H** IHC showing reduced S100β + (**F**), SOX9+ (**G**), and GFAP+ (**H**) cells in the CRS mice ($n = 6$ replicates). **I**, **J** RT–PCR and WB analyses showing that PTN mRNA (**I**) and PTN protein expression (**J**) were reduced in CRS mice ($n = 6$ mice per group). **K** IHC showing reduced PTN+ cells in the dmPFC of CRS mice ($n = 6$ replicates). **L** Representative images of PTN+ (red) and S100β + (green) co-stained cells (upper panel), PTN+ (green) and SOX9+ (red) co-stained cells (middle panel), PTN+ (green) and GFAP+ (red) co-stained cells (lower panel) ($n = 6$ replicates). **M** WB analysis showing reduced PTN within isolated astrocytes in the CRS mice ($n = 6$ mice per group). **N**–**P** Traces of mEPSCs in CaMKIIα+ neurons from the indicated groups (**N**), and quantification of the amplitude (**O**) and frequency (**P**) between groups ($n = 30$ cells from 10 mice per group). **Q** Traces of action potentials in CaMKIIα+ neurons and the corresponding statistical analysis ($n = 30$ cells from 10 mice per group). **R** Quantification of PSD95 expression ($n = 6$ mice per group). **S** Traces of dendritic spines in CaMKIIα+ neurons and quantification of the density ($n = 30$ cells from 10 mice per group). Diagrams of mouse CRS model and mouse brain in (**A**) were created in BioRender. chi, d. (2025) https://BioRender.com/x64m191. All data are presented as mean ± SEM. $^{*}P < 0.05$, $^{**}P < 0.01$, $^{***}P < 0.001$. See Supplementary Data 5 for statistical details, including the statistical test used for data analysis and the exact P value. Source data are provided as a Source Data file.

(Fig. 7L), decreased dendritic spine density (Fig. 7M), and diminished PSD95 expression (Fig. 7N). These findings suggest that PTPRZ1 in excitatory neurons may also exert antidepressant effects.

Next, we investigated the interaction between the astrocytic PTN and PTPRZ1 in excitatory neurons in the dmPFC. After specifically knocking down PTPRZ1 in excitatory neurons, exogenous PTN or vehicle was administered to the dmPFC of WT mice (Fig. 7O). We found that the depletion of PTPRZ1 induced depression-related behaviors in WT mice, whereas subsequent exogenous PTN administration caused no significant changes in these behaviors (Fig. 7P). Moreover, the administration of PTN failed to restore neuronal excitability (Fig. 7Q–T) or enhance neuronal synaptic transmission (Fig. 7U, V) when PTPRZ1 in excitatory neurons was depleted. In addition, we selectively overexpressed astrocytic PTN in the dmPFC of Aldh1l1-Cre/ERT2 mice after PTN was knocked down with CMV-PTN-shRNA, and the Aldh1l1-Cre/ERT2 mice greatly recovered from depression-related behaviors with the subsequent upregulation of astrocytic PTN (Supplementary Fig. 9A, B). The Co-IP experiment was conducted to demonstrate the interaction between PTN and PTPRZ1 (Supplementary Fig. 9D). Overall, the results revealed that the astrocytic PTN in the dmPFC interacts with PTPRZ1 in excitatory neurons to mediate antidepressant effects.

https://doi.org/10.1038/s41467-025-57924-1

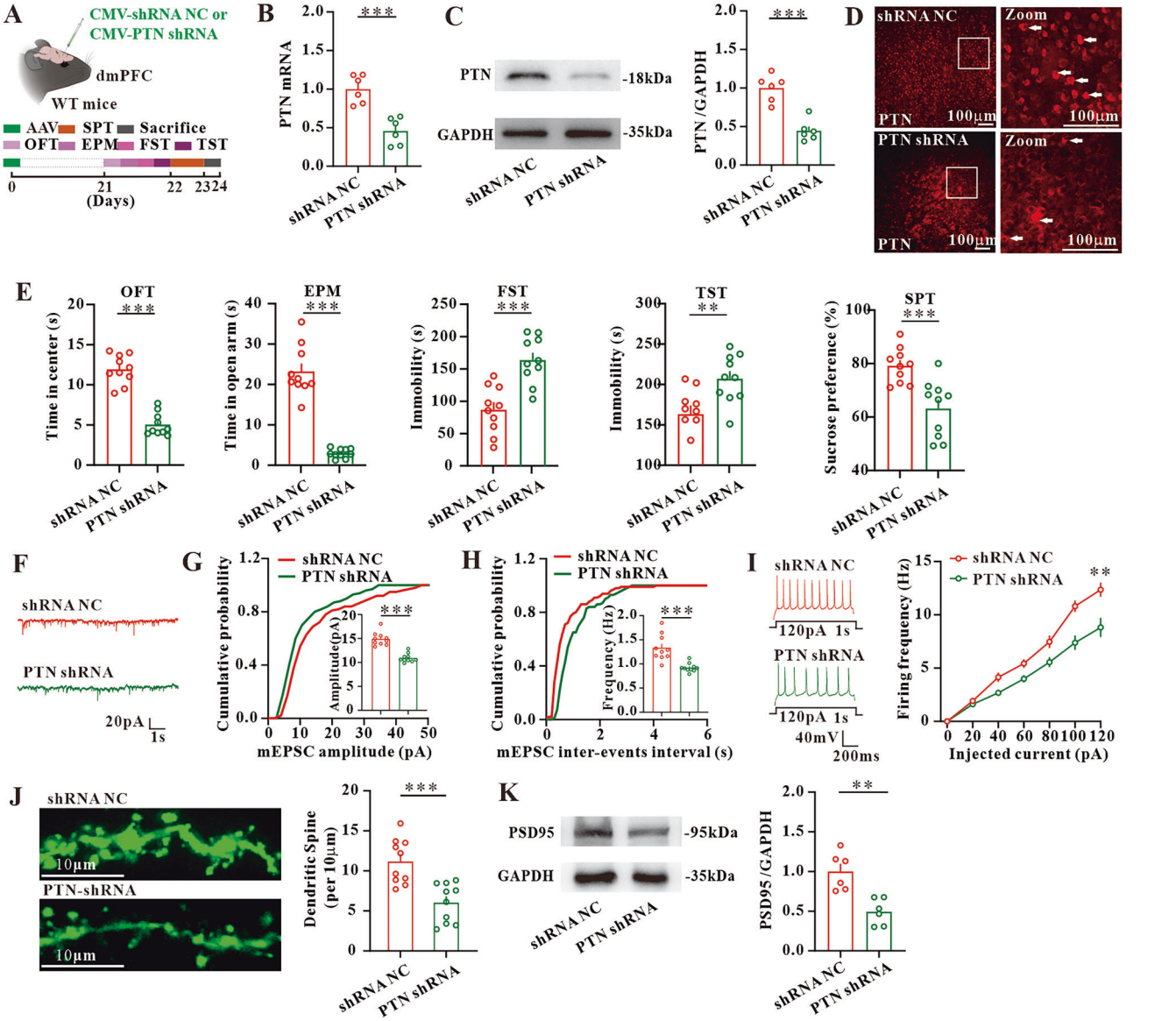

Fig. 4 | Knockdown of the PTN in the dmPFC promotes depression-related behaviors, reduces neuronal excitability, and leads to synaptic impairment. **A** Schematic of the experimental design (WT mice). **B**–**D** RT–PCR (**B**, $n = 6$ mice per group), WB (**C**, $n = 6$ mice per group), and IHC (**D**, $n = 6$ replicates) analyses showing the knockdown efficiency of AAV-PTN-shRNA. **E** Analyses of behavioral tests, including the OFT, EPM, FST, TST, and SPT ($n = 10$ mice per group). **F**–**H** Traces of mEPSCs in CaMKIIα+ neurons from the indicated groups (**F**), and the statistical analysis of the amplitude (**G**) and frequency (**H**) between groups ($n = 30$ cells from 10 mice per group). **I** Traces of action potentials in CaMKIIα+ neurons from the indicated groups and the corresponding statistical analysis ($n = 30$ cells from 10 mice per group). **J** Traces of dendritic spines from CaMKIIα+ neurons and quantification of the density of dendritic spines ($n = 30$ cells from 10 mice per group). **K** Quantification of PSD95 expression ($n = 6$ mice per group). Diagrams of the mouse injection model and mouse brain in (**A**) were created in BioRender. chi, d. (2025) https://BioRender.com/x64m191. All data are presented as mean ± SEM. $^{**}P < 0.01$, $^{***}P < 0.001$. See Supplementary Data 5 for statistical details, including the statistical test used for data analysis and the exact *P* value. Source data are provided as a Source Data file.

Astrocytic PTN in the dmPFC interacts with PTPRZ1 in excitatory neurons to mediate antidepressive effects by activating the AKT signaling pathway

To investigate the downstream molecular mechanisms underlying PTN-PTPRZ1 signaling in MDD, we next conducted a NicheNet analysis, a cell–cell communication tool that can predict the responsive target genes involved in altered ligand–receptor interactions (Supplementary Fig. 5A–E). The NicheNet results predicted 92 target genes following the PTN-PTPRZ1 pair (Supplementary Fig. 5E). Pathway enrichment of these target genes revealed that the downstream pathways were related to kinase activity, kinase binding, and activation of protein kinase activity (Fig. 8A). Furthermore, GSEA of DEGs in excitatory neurons, the effector cells executing pathway functions, revealed a decrease in PI3K-AKT-MTOR signaling in the suicide group (Fig. 8B). Previous studies have reported that PTN regulates adult neurogenesis by binding to PTPRZ1 to activate the AKT signaling pathway[44]. Collectively, these results indicate that the AKT signaling pathway may serve as a downstream target of PTN-PTPRZ1 activity in astrocyte-to-excitatory neuron communication.

We first examined the level of AKT within the dmPFC in WT mice subjected to CRS. WB analysis revealed that the level of phosphorylated AKT (p-AKT) was significantly reduced in the CRS mice, whereas no obvious differences in total AKT were detected (Fig. 8C). We applied SC79, an activator of AKT, to the dmPFC of WT CRS mice (Fig. 8D). SC79 significantly improved depression-related behaviors (Fig. 8E), increased the amplitude and frequency of mEPSCs

https://doi.org/10.1038/s41467-025-57924-1

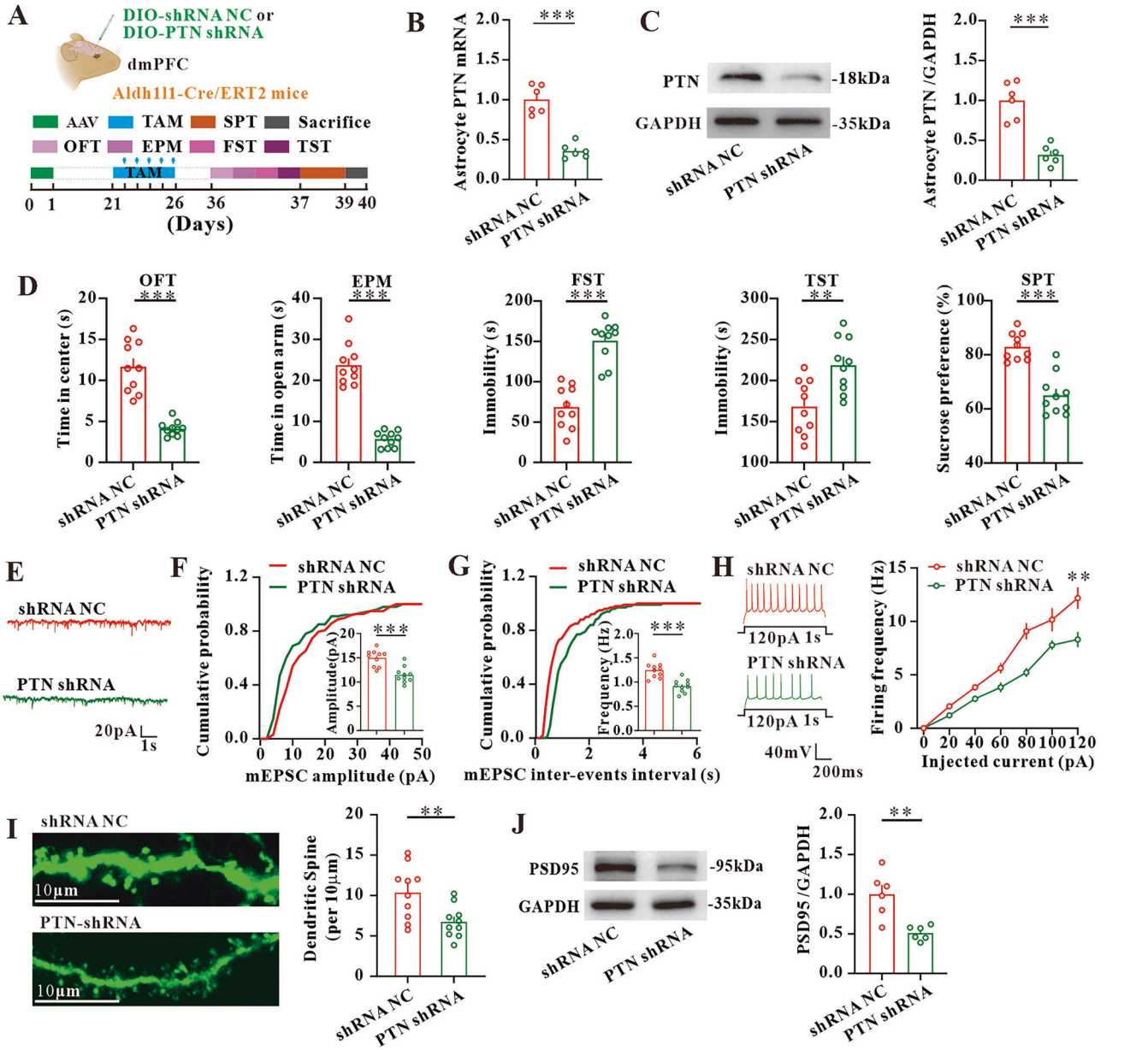

Fig. 5 | Astrocytic PTN in the dmPFC modulates depression-related behaviors and neuronal excitability and synaptic functions. A Schematic of the experimental design (Aldh1l1-Cre/ERT2 mice). **B**, **C** Validation of the knockdown efficiency of DIO-PTN-shRNA in Aldh1l1-Cre/ERT2 mice through RT–PCR analysis of PTN mRNA (**B**) and WB analysis of PTN protein (**C**) in astrocytes isolated from the dmPFC ($n = 6$ mice per group). **D** Analyses of behavioral tests, including the OFT, EPM, FST, TST, and SPT ($n = 10$ mice per group). **E**–**G** Traces of mEPSCs in CaMKIIα+ neurons in Aldh1l1-Cre/ERT2 mice from the indicated groups (**E**), and the statistical analysis of the amplitude (**F**) and frequency (**G**) of mEPSCs between groups ($n = 30$ cells from 10 mice per group). **H** Traces of action potentials in CaMKIIα+ neurons in Aldh1l1-Cre/ERT2 mice from the indicated groups and the corresponding statistical analysis ($n = 30$ cells from 10 mice per group). **I** Traces of dendritic spines from CaMKIIα+ neurons in Aldh1l1-Cre/ERT2 mice and quantification of the density ($n = 30$ cells from 10 mice per group). **J** Quantification of PSD95 expression ($n = 6$ mice per group). Diagrams of the mouse injection model and mouse brain in (**A**) were created in BioRender. chi, d. (2025) https://BioRender.com/x64m191. All data are presented as mean ± SEM. $^{**}P < 0.01$, $^{***}P < 0.001$. See Supplementary Data 5 for statistical details, including the statistical test used for data analysis and the exact *P* value. Source data are provided as a Source Data file.

(Fig. 8F–H), potentiated the firing rates of action potentials (Fig. 8I), and increased the density of dendritic spines (Fig. 8J), demonstrating the potential antidepressant effects of the AKT pathway. Similar results in depression-related behavioral tests were found in the WT CSDS mouse model (Supplementary Fig. 8C). Next, we explored the relationship between the PTN-PTPRZ1 pathway and AKT signaling. To examine whether PTPRZ1 depletion or exogenous PTN infusion affects AKT signaling, we conducted a series of experiments with WT mice (Fig. 8K). WB analysis revealed that exogenous PTN infusion in the dmPFC increased p-AKT, whereas PTPRZ1 knockdown in excitatory neurons reduced p-AKT expression (Fig. 8L, M). However, administering PTN in the dmPFC failed to alter p-AKT expression when PTPRZ1 in excitatory neurons had already been inhibited (Fig. 8L, M). We then applied MK2206, an inhibitor of AKT, to the dmPFC of WT mice (Fig. 8N). MK2206 administration induced depression-related behaviors (Fig. 8O), reduced the amplitude and frequency of mEPSCs (Fig. 8P–R), decreased the firing rates of action potentials (Fig. 8S), and decreased the density of dendritic spines (Fig. 8T). These results suggest that PTN-PTPRZ1 in the dmPFC modulates depression responses by activating the AKT signaling pathway.

https://doi.org/10.1038/s41467-025-57924-1

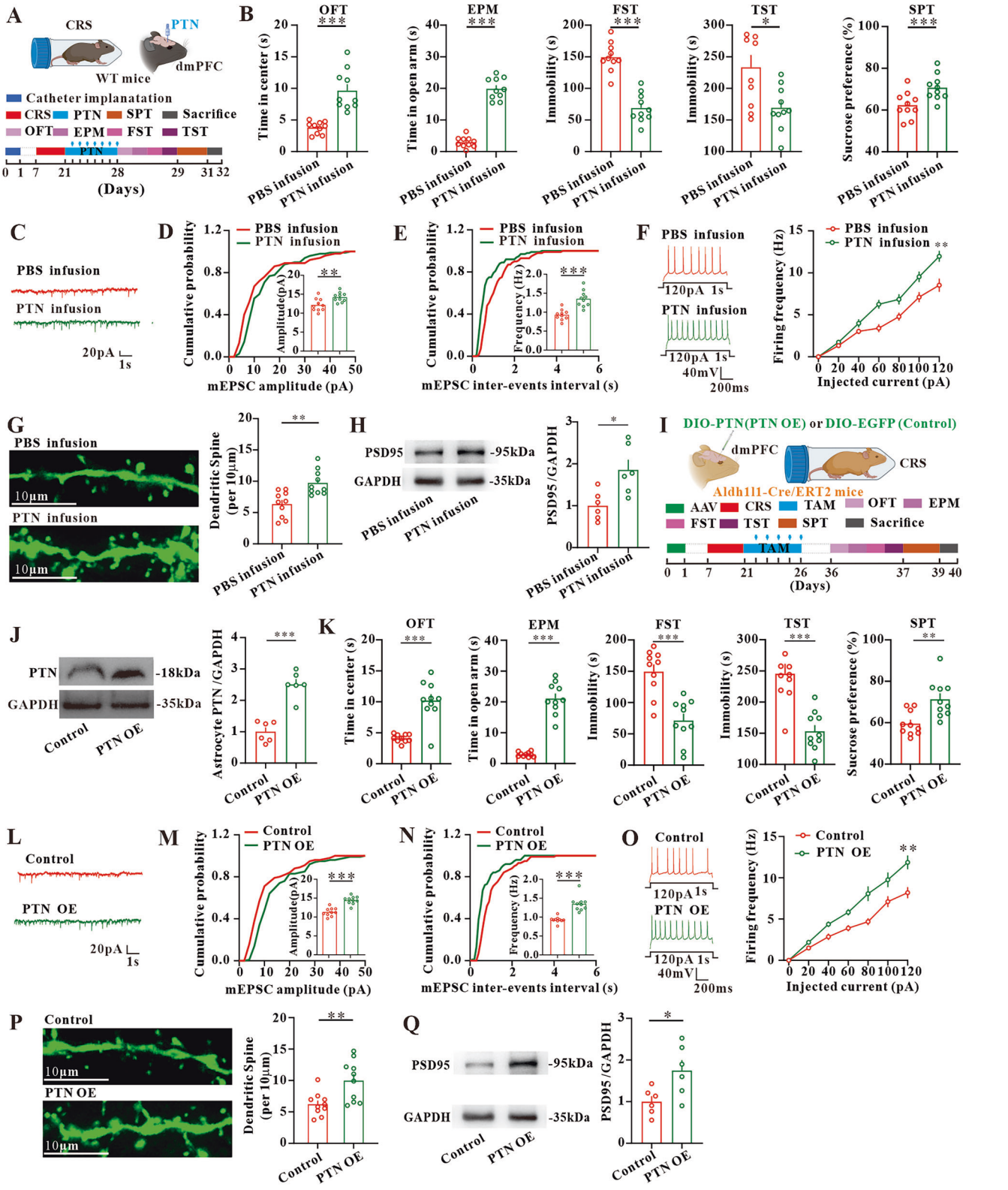

Discussion

In this study, through snRNA-seq data and CellChat analyses, we found that the proportion of astrocytes in the dlPFC was decreased and that the PTN signaling pathway involved in astrocyte-to-excitatory neuron communication was attenuated in male MDD patients compared with mentally healthy controls. In vivo experiments revealed that reduced numbers of astrocytes and diminished PTN expression in the dmPFC were detected in a male mouse model of depression induced by CRS and CSDS. Furthermore, PTN from astrocytes in the dmPFC modulated depression-related responses. The knockdown of astrocytic PTN induced depression-related behaviors, reduced neuronal excitability, and impaired synaptic function, which was reversed by supplementation with exogenous PTN or the upregulation of astrocytic PTN in the dmPFC. Moreover, astrocytic PTN exerted antidepressant effects via interaction with PTPRZ1 in excitatory neurons and further activation of the AKT signaling pathway.

Fig. 6 | PTN infusion alleviates depression-related behaviors in CRS-susceptible mice. A Schematic of the experimental design (WT mice). **B** Analyses of behavioral tests, including the OFT, EPM, FST, TST, and SPT ($n = 10$ mice per group). **C**–**E** Traces of mEPSCs recorded in CaMKIIα+ neurons (**C**), and the statistical analysis of the amplitude (**D**) and frequency (**E**) between groups ($n = 30$ cells from 10 mice per group). **F** Traces of action potentials in CaMKIIα+ neurons from the indicated groups and the corresponding statistical analysis ($n = 30$ cells from 10 mice per group). **G** Traces of dendritic spines from CaMKIIα+ neurons and quantification of the density ($n = 30$ cells from 10 mice per group). **H** Quantification of PSD95 expression ($n = 6$ mice per group). **I** Schematic of the experimental design (Aldh1l1-Cre/ERT2 mice). **J** Validation of AAV transfection efficiency via quantification of PTN expression in isolated astrocytes ($n = 6$ mice per group). **K** Analyses of behavioral tests, including the OFT, EPM, FST, TST, and SPT ($n = 10$ mice per group). **L**–**N** Traces of mEPSCs in CaMKIIα+ neurons from the indicated groups (**L**), and quantification of the amplitude (**M**) and frequency (**N**) ($n = 30$ cells from 10 mice per group). **O** Traces of action potentials in CaMKIIα+ neurons from the indicated groups and the corresponding statistical analysis ($n = 30$ cells from 10 mice per group). **P** Traces of dendritic spines in CaMKIIα+ neurons from the indicated groups and quantification of the density ($n = 30$ cells from 10 mice per group). **Q** Quantification of PSD95 expression ($n = 6$ mice per group). Diagrams of mouse injection model, CRS model, and mouse brain in (**A**, **I**) were created in BioRender. chi, d. (2025) https://BioRender.com/x64m191. All data are presented as mean ± SEM. $^{*}P < 0.05$, $^{**}P < 0.01$, $^{***}P < 0.001$. See Supplementary Data 5 for statistical details, including the statistical test used for data analysis and the exact P value. Source data are provided as a Source Data file.

Astrocytes play a crucial role in the pathology of MDD, as astrocytes regulate glutamatergic neurotransmission, modulate neural and synaptic plasticity through the secretion of growth factors such as brain-derived neurotrophic factor (BDNF), and mediate neuroinflammation[49]. Postmortem studies indicate that both the frequency and severity of reactive astrogliosis are reduced in the brains of individuals with MDD[50]. Our results also revealed that the density of astrocytes in the dmPFC was significantly reduced in a mouse model of depression induced by CRS and CSDS. We utilized S100β, SOX9, and GFAP as the markers for astrocytes, and all markers demonstrated a reduction of astrocyte number in the dmPFC of mice under chronic stress. Andrea et al. reported that unpredictable chronic mild stress followed by social isolation increased GFAP immunoreactivity and increased s100β-positive cell density in the dentate gyrus of the hippocampus in mice[51]. This discrepancy is likely due to the different mouse models and different brain regions used in the two studies. In addition, in Andrea's study[51], the tendency of GFAP-positive cell immunoreactivity and cell density in the PFC was not in accordance with that in the dentate gyrus. Astrocytes play a vital role in regulating the transmission of glutamate, and glutamate serves as a key messenger facilitating communication between central neurons and astrocytes[52]. Repair of impaired astrocyte function can affect antidepressant effects by ensuring neuronal activity[53]. Mice that have diminished expression of the glutamate transporter GLT-1 in astrocytes of the habenula are more prone to stress and show heightened immobility in tail-suspension tests[54]. These observations support the importance of preserving the function of astrocytes in MDD treatment.

PTN, also known as heparin-binding growth-associated molecule, is an extracellular matrix protein that plays important roles in neurite outgrowth, synaptogenesis, and synaptic plasticity[55,56]. PTN is closely associated with neuroplasticity, and PTN can mediate newborn neuron development through activation of the AKT signaling pathway[37]. PTN can exert protective effects on the development of addictive and neurodegenerative diseases such as Parkinson's disease and Alzheimer's disease[57]. The pathogenesis of MDD is related to impaired excitation–inhibition balance within neurons in the central nervous system[58]. The clearance of glutamate, which affects neuronal excitability and the strength of glutamatergic synapses, contributes to depression[59]. As the main excitatory neurotransmitter released by synapses, glutamate is involved in synaptic plasticity, cognitive processes, and reward and emotional processes. Stress can affect the presynaptic secretion of glutamate and activate downstream signaling pathways by binding to receptors on the postsynaptic membrane[60]. The impairment of glutamatergic neuron function is involved in the development of depression, and the regulation of the glutamatergic system affects depression-related responses[61,62]. Astrocytes are capable of adjusting the strength of synapses by enhancing spontaneous excitatory postsynaptic currents[63]. This finding is consistent with our findings in the present study. The knockdown of the astrocytic PTN in the dmPFC results in a decreased firing frequency in excitatory neurons, a reduced amplitude and frequency of mEPSCs, diminished dendritic spine density, and decreased PSD95 expression, indicating attenuated neuronal excitability and hypoactive synaptic functions. The reduced astrocytic PTN in the dmPFC induced depression, possibly due to the impairment of neuronal excitability and glutamatergic transmission.

As a member of the transmembrane protein tyrosine phosphatase family, PTPRZ1 belongs to the PTN receptor family and binds to PTN through its extracellular domain[64]. The role of PTN-PTPRZ1 in several central nervous system diseases has been studied[65,66]. Potentiation of the PTN-PTPRZ1 pathway in the hippocampus activates AKT signaling, resulting in the restoration of neurogenesis and alleviation of memory deficits in aging mice[44]. PTN-PTPRZ1 signaling promotes oligodendrocyte precursor cell proliferation and differentiation during developmental myelination and remyelination after injury. PTPRZ1 is also highly expressed in glial cells of the central nervous system, including astrocytes and oligodendrocytes[65]. However, whether PTPRZ1 in astrocytes affects the development of MDD in the same way as it does in excitatory neurons in our study is not yet clear. The astrocytic PTN in the dmPFC may mediate the progression of MDD via interactions with not only PTPRZ1 in excitatory neurons but also PTPRZ1 in astrocytes; however, more experiments are needed to clarify these effects. The role of the AKT pathway in depression has been widely studied. The regulation of downstream AKT signaling facilitates the amelioration of depression-related behaviors[67,68]. The neurotrophic factor brain-derived neurotrophic factor (BDNF) can mediate the AKT pathway to improve synaptic plasticity and exert antidepressant effects[69]. These observations are consistent with our finding that the activation of phosphorylated AKT by the PTN-PTPRZ1 interaction can exert antidepressant effects.

There are some limitations in our study. First, the current study focused on male MDD patients and male mice, mainly because the prevalence, symptoms, and molecular signatures of MDD differ by sex[70–72] and we think it is more reasonable to analyze these factors separately. The effect of PTN-PTPRZ1 pathway on female subjects with depression needs further verification. Second, direct evidence demonstrating the interaction between astrocytic PTN and neuronal PTPRZ1 was not presented in this study, and more experiments are needed to confirm that interaction in the future. Third, we found that the phosphorylation of AKT was affected by the aberrant expression of astrocytic PTN and neuronal PTPRZ1 and that interfering with AKT activity through exogenous administration of an AKT activator or inhibitor mediated the depression-related responses. However, the intervention measures we utilized lacked cell type specificity. Fourth, Li X et al. reported that tamoxifen caused negative effects on the behaviors of mice[73], whereas our results showed that the administration of tamoxifen had no significant effects on the observed behaviors. The discrepancy may be due to differences in the total dosage of tamoxifen administration between the two studies. As the main plasma active metabolite of tamoxifen, 4-hydroxytamoxifen can effectively shorten the time to exert effects and reduce the frequency of drug administration, which can possibly reduce the side effects of

https://doi.org/10.1038/s41467-025-57924-1

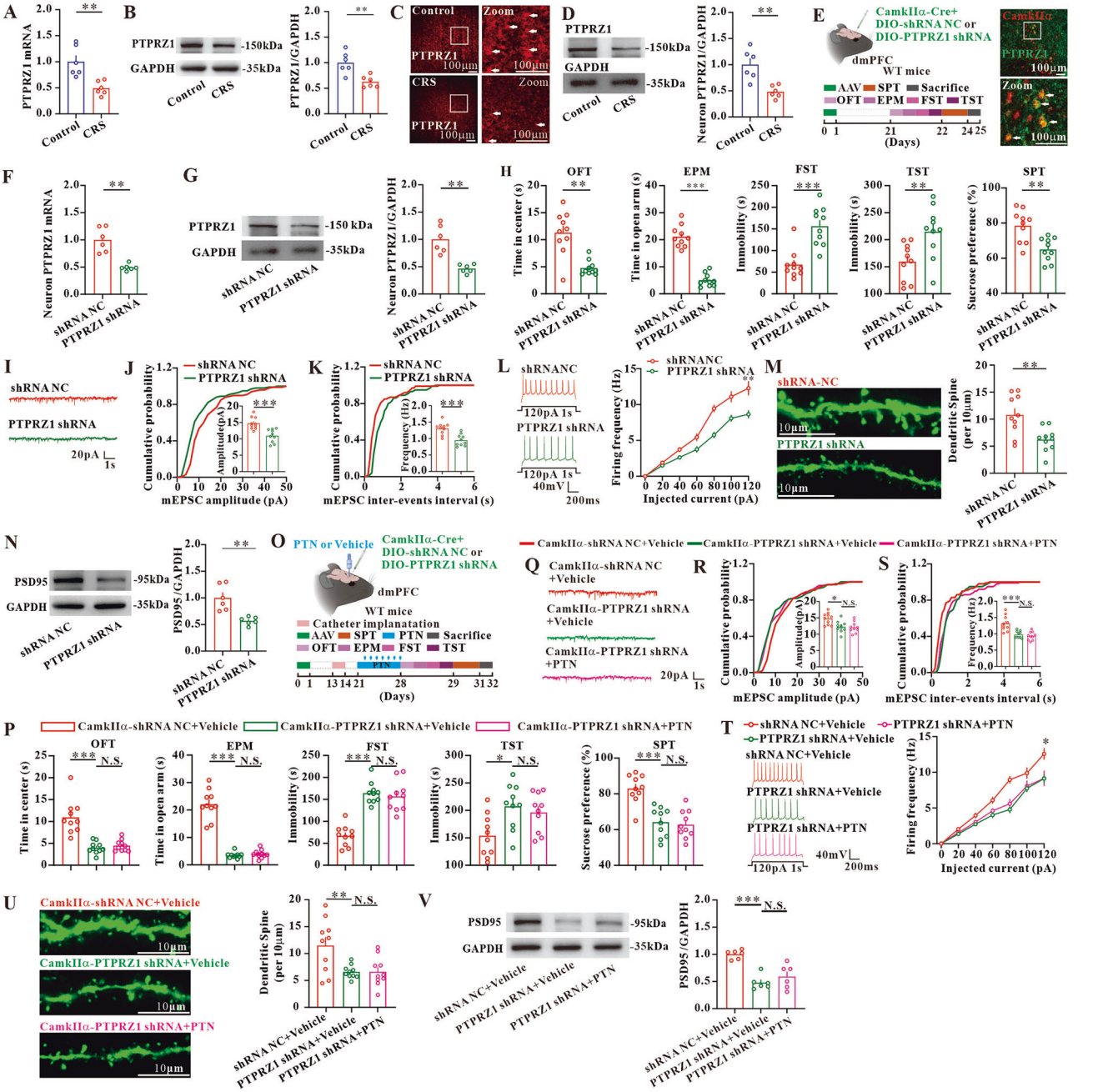

Fig. 7 | Astrocytic PTN within dmPFC interacts with PTPRZ1 in excitatory neurons to mediate antidepressant effects. A–C Quantification of PTPRZ1 mRNA (**A**) and protein (**B**) ($n = 6$ WT mice per group), and verification by IHC analysis (**C**) ($n = 6$ replicates). **D** Quantification of isolated neuronal PTPRZ1 ($n = 6$ WT mice per group). **E** Schematic of the experimental diagram (WT mice) and IHC showing PTPRZ1 (green) co-expressed with CaMKIIα + (red) neuron ($n = 6$ replicates). **F, G** Validation of DIO-PTPRZ1-shRNA through quantification of PTPRZ1 mRNA (**F**) and protein (**G**) ($n = 6$ mice per group). **H** Behavioral tests analyses, including OFT, EPM, FST, TST, and SPT ($n = 10$ mice per group). **I–K** Traces of mEPSCs in CaMKIIα+ neurons (**I**), and quantification of amplitude (**J**) and frequency (**K**) ($n = 30$ cells from 10 mice per group). **L** Traces and quantification of action potentials in CaMKIIα+ neurons ($n = 30$ cells from 10 mice per group). **M** Traces and quantification of dendritic spines from CaMKIIα+ neurons ($n = 30$ cells from 10 mice per group). **N** Quantification of PSD95 ($n = 6$ mice per group). **O** Schematic of experimental design (WT mice). **P** Behavioral tests analyses, including OFT, EPM, FST, TST, and SPT ($n = 10$ mice per group). **Q–S** Traces of mEPSCs in CaMKIIα+ neurons (**Q**), and quantification of amplitude (**R**), and frequency (**S**) ($n = 30$ cells from 10 mice per group). **T** Traces and quantification of action potentials from CaMKIIα+ neurons ($n = 30$ cells from 10 mice per group). **U** Traces and quantification of dendritic spines from CaMKIIα+ neurons ($n = 30$ cells from 10 mice per group). **V** Quantification of PSD95 ($n = 6$ mice per group). Diagrams of the mouse brain and injection model in (**E**, **O**) were created in BioRender. chi, d. (2025) https://BioRender.com/x64m191. All data are presented as mean ± SEM. N.S. = not significant, $^*P < 0.05$, $^{**}P < 0.01$, $^{***}P < 0.001$. See Supplementary Data 5 for statistical details, including the statistical test used for data analysis and the exact *P* value. Source data are provided as a Source Data file.

tamoxifen to a greater extent. Using 4-hydroxytamoxifen might be a better choice for future experiments.

In summary, astrocytic PTN in the dmPFC functions as a critical regulator of depression-related behaviors in a male mouse model of depression induced by CRS and CSDS. Astrocytic PTN in the dmPFC interacts with PTPRZ1 in the CaMKIIα+ excitatory neurons to modulate neuronal excitability and synaptic transmission, which further activates the AKT signaling pathway to exert antidepressant effects. These

https://doi.org/10.1038/s41467-025-57924-1

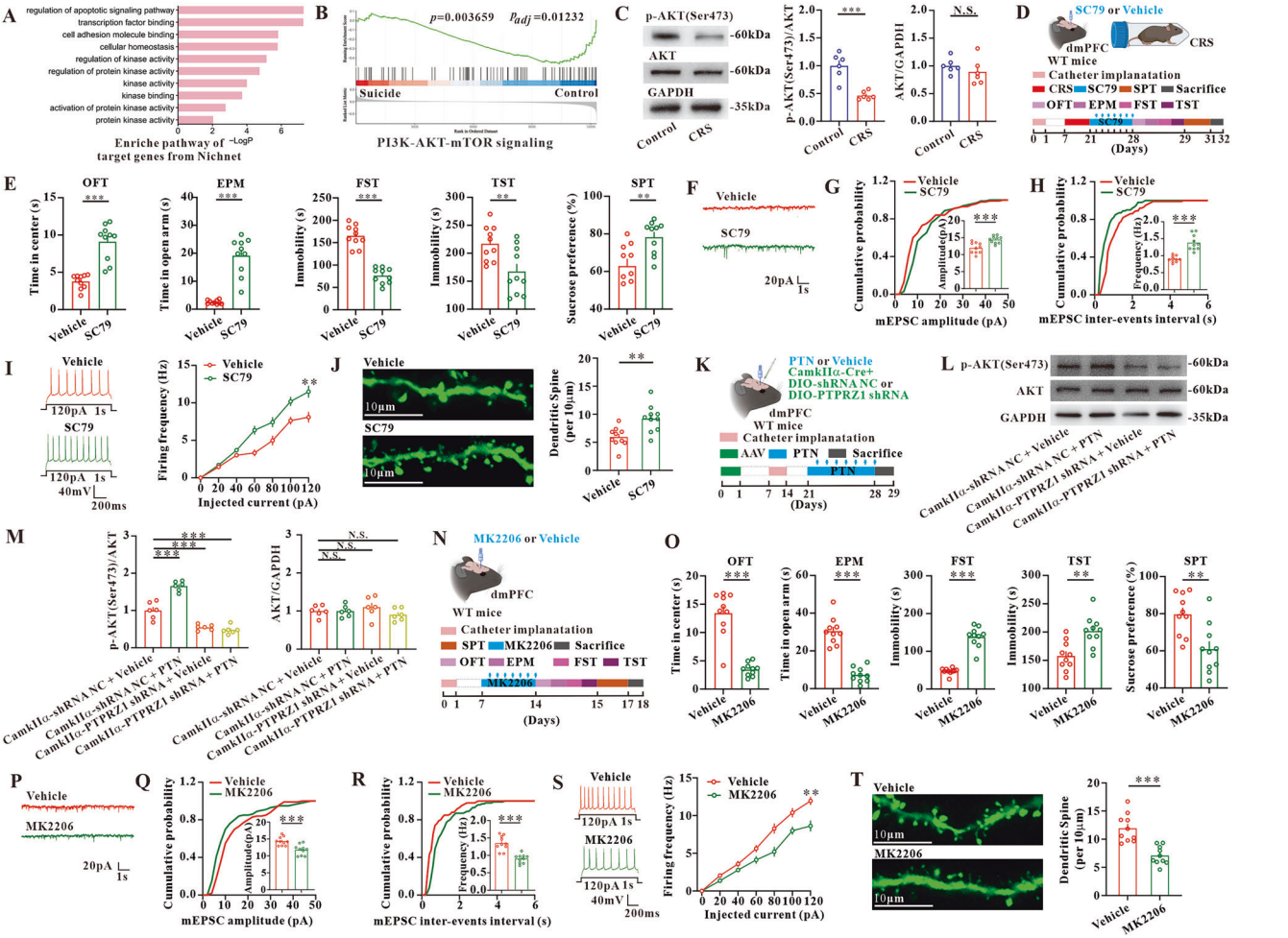

Fig. 8 | Astrocytic PTN interacts with PTPRZ1 in excitatory neurons to mediate antidepressant effects by activating the AKT signaling pathway. A Bar plot of the GO pathway enrichment analysis showing the downregulated signaling pathways of target genes predicted from NicheNet. **B** GSEA results of excitatory DEGs showing the enrichment of PI3K_AKT_MTOR_signaling was attenuated in the suicide group. **C** Quantification of p-AKT and total AKT expression ($n = 6$ WT mice per group). **D** Schematic of experimental design (WT mice). **E** Analyses of behavioral tests, including the OFT, EPM, FST, TST, and SPT ($n = 10$ mice per group). **F**–**H** Traces of mEPSCs recorded from CaMKIIα+ neurons (**F**), and quantification of the amplitude (**G**) and frequency (**H**) ($n = 30$ cells from 10 mice per group). **I** Traces and quantification of action potentials from CaMKIIα+ neurons ($n = 30$ cells from 10 mice per group). **J** Traces of dendritic spines from CaMKIIα+ neurons and quantification of the density ($n = 30$ cells from 10 mice per group). **K** Schematic of the experimental design (WT mice). **L**, **M** Quantification of p-AKT and total AKT expression ($n = 6$ mice per group). **N** Schematic of experimental design (WT mice). **O** Analyses of behavioral tests, including the OFT, EPM, FST, TST, and SPT ($n = 10$ mice per group). **P**–**R** Traces of mEPSCs recorded from CaMKIIα+ neurons (**P**), and quantification of the amplitude (**Q**), and frequency (**R**) ($n = 30$ cells from 10 mice per group). **S** Traces and quantification of action potentials from CaMKIIα+ neurons ($n = 30$ cells from 10 mice per group). **T** Traces of dendritic spines from CaMKIIα+ neurons and quantification of the density ($n = 30$ cells from 10 mice per group). Diagrams of the mouse, mouse brain and CRS model in (**D**, **K**, **N**) were created in BioRender. chi, d. (2025) https://BioRender.com/x64m191. All data are presented as mean ± SEM. N.S. = not significant, $^{**}P < 0.01$, $^{***}P < 0.001$. See Supplementary Data 5 for statistical details, such as the statistical test used for data analysis and the exact *P* value. Source data are provided as a Source Data file.

findings highlight the PTN-PTPRZ1-AKT axis in astrocyte-to-excitatory neuron communication as a promising therapeutic target for MDD.

Methods

Dataset acquisition and study participants

The processed MDD single-nucleus RNA sequencing data from GBM samples (GSE144136) were obtained from the Gene Expression Omnibus (GEO, http://www.ncbi.nlm.nih.gov/geo/) database, and the GWAS summary statistics for MDD patients (170,756 cases and 329,443 controls) were obtained from the IEU OpenGWAS (https://gwas.mrcieu.ac.uk/) database with a GWAS ID of ieu-b-102. The published MDD cohort[48] consisted of 17 male patients and controls. Cases met the diagnostic criteria for MDD and died by suicide, whereas individuals in the control group died by accident ($n = 6$) or natural causes ($n = 11$). Postmortem brain samples were dissected from Brodmann area 9 (dlPFC), and snRNA sequencing was performed (Supplementary Data 1).

Single-cell data processing and cell clustering

We downloaded the processed snRNA sequencing data from the GEO dataset, which had been aligned and quantified using the Cell Ranger Single-Cell Software Suite (10X Genomics Cellranger v2.1.0). The gene expression data were also mapped to the human genome (GRCh38-1.2.0). For the quality check procedure, we first removed the cluster cells originally labeled "Mix" from the dataset. Next, any cells were removed if they expressed fewer than 201 genes or if more than 20% of the UMIs were linked to mitochondrial genes[74,75]. To eliminate batch effects, the R package Harmony (version 1.2.0) was used to remove batch correction before clustering analysis. Other steps, including Seurat object creation, data normalization, data scaling, identification of variable genes, dimensional reduction, clustering, and UMAP projection, were performed following the standard pipeline of the Seurat R package (version 4.4.0, https://satijalab.org/seurat).

Cluster annotation

All the nuclei were annotated as distinct major cell types on the basis of the average gene expression of known canonical marker genes, including excitatory neurons (markers: SATB2, SLC17A7, and CAMK2A), inhibitory neurons (GAD1 and GAD2), astrocytes (GFAP, AQP4, GLUL, SOX9, GJA1, NDRG2, and ALDH1A1), oligodendrocytes (MBP, PLP1, MOBP, and MAG), oligodendrocyte precursor cells (PCDH15, PDGFRA, OLIG1, OLIG2, and PTGDS), endothelial cells (CLDN5 and VTN), and microglia/macrophage (CX3CR1, MRC1, SPI1, and TMEM119) cells. In addition, SNAP25, STMN2, and RBFOX3 were used as common neuron markers across all the neuronal populations.

We further identified subclusters and annotated them as specific cell subtypes within excitatory and inhibitory neurons on the basis of the average expression of the corresponding gene sets. The marker genes for each subcluster within the major cell types were identified using the FindAllMarkers function in the Seurat package. For excitatory neurons, subclusters were annotated according to layer-specific gene markers as follows: layers II–IV (CUX2, RASGRF2, and PVRL3), layer IV/V (RORB), layer V (SULF2, PCP4, and HTR2C), layers V/VI (TOX, ETV1, RXFP1, and FOXP2), and layer VI (NR4A2, SYNPR, TLE4, and NTNG2). For inhibitory neurons, subclusters were annotated on the basis of well-known markers, including CCK, CALB, VIP, SST, PVALB, SLC32A1, and DLX.

Differential expression analysis

Analysis of differentially expressed genes (DEGs) for key ligands and receptors between the suicide and control groups was performed using two-sided Wilcoxon tests within each responding cluster, with Benjamini–Hochberg correction applied to adjust *P* values for multiple testing. A BH-adjusted *P* value less than 0.05 was considered statistically significant. Additionally, the jjVolcano function from the scRNAtoolVis package (version 0.0.7) was used to visualize DEGs in a Manhattan plot between the suicide and control groups across all clusters.

Group preference of each cell type

To quantify the cell type enrichment across groups, we compared the observed to expected cell numbers in each type according to the following formula as we described previously[76,77]:

$$Ro/e = \frac{observed}{expected} \quad (1)$$

where the expected cell numbers for each combination of cell types and groups are obtained via the chi-square test. Ro/e is the ratio of observed to expected cell numbers in each cell type. Ro/e > 1 suggests a preference for this cell type in this group, and Ro/e < 1 suggests that cells of the given cell type are observed with less frequency than random expectations in the specific group.

Cell–cell interaction analysis

CellChat. To compare differences in cell–cell communication networks across different sources, we utilized CellChat (version 1.6.1, https://github.com/sqjin/CellChat)[78]. The normalized expression data, preprocessed using Seurat, were input into CellChat for downstream analysis. We applied standard preprocessing functions with default parameters, including identifyOverExpressedGenes, identifyOverExpressedInteractions, and projectData, to identify significantly overexpressed genes and interactions and project the data onto inferred interaction networks. We subsequently ran the core functions computeCommunProb, computeCommunProbPathway, and aggregateNet using default settings to compute the communication probabilities and aggregate the interaction networks. The MDD and control groups were merged for further analysis using computeNetSimilarityPairwise, allowing pairwise comparisons of network differences. To visualize the communication patterns, the functions compareInteractions, rankNet, and netVisual_bubble were used.

Initially, we performed CellChat analysis of all the nuclei and determined that excitatory neurons were most regulated by astrocytes. We then subset the relevant nuclei from excitatory neurons and astrocytes for a more focused CellChat analysis followed by the abovementioned steps.

NicheNet. We used NicheNet (version 2.1.7, https://github.com/saeyslab/nichenetr)[79] to infer interactions between astrocytes and excitatory neurons, designating astrocytes as "Sender" cells and excitatory neurons as "Receiver" cells. Only genes expressed in more than 10% of the cells within clusters were considered for further ligand–receptor interaction analysis. We extracted ligands with upregulated activity that overlapped with the CellChat results from the control vs. suicide comparison (i.e., ligands with downregulated activity in the suicide group compared with the control group) and the top 1000 targets from the differentially expressed genes of the "Sender" and "Receiver" cells for paired ligand–receptor activity analysis. The ligand_activity_target_heatmap function was applied to visualize ligand regulatory activity, with activity scores ranging from 0 to 1. In addition, a heatmap was generated to illustrate the expression of differentially expressed ligands and receptors, which was calculated by averaging gene expression in the relevant cell populations and scaling across the indicated clusters.

Pathway enrichment analysis

Gene ontology (GO) analysis. To perform GO analysis, the potential target genes of excitatory neurons regulated by astrocytes through the PTN pathway, as predicted by NicheNet, were analyzed using the online tool Metascape[80] (http://metascape.org/gp/index.html) to identify the enriched pathways. Only gene sets in the "GO Biological Processes", "GO Molecular Functions" and "GO Cellular Components" categories were considered, and a *P* value less than 0.05 was considered statistically significant.

Gene set enrichment analysis (GSEA). To explore the potential downstream signaling pathways affected by PTN signaling, we conducted GSEA using GSEABase (version 1.64.0) and gene sets from the Molecular Signatures Database (https://www.gsea-msigdb.org/gsea/msigdb/human/collections.jsp)[81]. The DEGs in excitatory neurons between the suicide and control groups were subjected to GSEA. Genes were ranked by log2-fold change from the differential expression analysis, GSEA was conducted using hallmark (H) and curated (C2) gene sets with 1000 permutations, and a *P* adjusted value less than 0.05 was considered statistically significant.

Pathway-based polygenic regression (scPagwas) to identify MDD-relevant clusters

To identify the genetic associations of cell clusters with MDD, we used scPagwas (https://dengchunyu.github.io/)[82], which uses an optimized polygenic regression model to integrate snRNA-seq and GWAS data. For GWAS data preparation, we downloaded the GWAS summary statistics for MDD from the IEU OpenGWAS database and conducted data pruning following the scPagwas guidelines, including GWAS data reprocessing, SNP extraction, plink, filtering of LD information and integration of the result files for chromosomes 1–22 with default parameters. For snRNA-seq preparation, we subset the normalized and scaled expression data from the suicide group. The prepared GWAS and snRNA-seq data were then input into scPagwas for downstream analysis, with 1000 top genes and 200 iterations specified.

Animals

Male C57/BL6 mice (8–10 weeks) were purchased from the Institute of Experimental Animals of Guangdong Medicine Experimental Animal

Center. Male Aldh1l1-Cre/ERT2 (Cat# 031008) mice (8–10 weeks) were purchased from the Jackson Laboratory. All the mice were housed on a standard 12-h light/dark cycle (light from 7 a.m. to 7 p.m.) at a constant temperature of 25 ± 1 °C and 50% humidity, with food and water available at all times. Ten mice per group were used in behavioral tests, electrophysiological recording, and dendritic spine analysis. Six mice per group were used in RT-PCR, western blotting (WB), and immunohistochemistry (IHC). All experimental procedures were approved by the Use Committee of Sun Yat-sen University Cancer Center and the Animal Care Committee (No. L102012024120D, No. L102012024228P) and were conducted in accordance with the guidelines of the National Institutes of Health (NIH).

Chronic restraint stress (CRS) model

The CRS model was established on the basis of procedures reported previously[83] with slight modifications. The mice were placed in well-ventilated 50-mL plastic tubes without food or water from 9:00 AM to 15:00 PM for 14 consecutive days. The plastic tubes prevented the mice from moving freely or turning around but did not squeeze the animals or cause any pain or physical injury. After being restrained, the mice were sent back to their home cages immediately. The mice that were not subjected to restraint were kept in their usual home cages without any restrictions for 14 days.

Chronic social defeat stress (CSDS) model and social interaction test (SIT)

CSDS was performed as followed[84]. Adult male CD-1 mice (4–6 months old) were used as aggressors. Before each defeat, aggressors were screened for aggressive behavior for 3 consecutive days. Two days before the start of defeat, the CD-1 mice were housed on one side of a perforated Plexiglass partition. During 10 consecutive days of CSDS, experimental mice (7–8 weeks old) were subjected to direct physical interaction with a CD-1 mouse for 10 min per day, and for the rest of the day were placed on the other side of the Plexiglass divider, allowing for sensory but not direct physical contact. The experimental mice were exposed to a new CD-1 aggressor every day for 10 days.

Before the SIT, the mice were placed in the behavioral suite and allowed to adapt for 1 h. After each test, the behavioral suite was cleaned with 75% alcohol to prevent odor interference. SIT was performed 24 h after CSDS modeling in a new CD-1 mouse. The test lasted for 5 min. The experimental mice were allowed to explore freely in the field (44 × 44 cm) in the first 2.5 min, where a rectangular container (10 × 6 cm) was placed. The CD-1 mice were placed in the container 2.5 min later and observed in the "interaction area" (14 × 26 cm). The statistical formula for the social interaction ratio was as follows: time in the interaction area when there was a CD-1 target mouse/time in the interaction area when there was no CD-1 target mouse × 100%.

Virus microinjection

Under continuous isoflurane inhalation anesthesia, the mice were placed in a stereotaxic frame (RWD Life Science Co., Ltd.), and the body temperature was maintained at 36 °C with a heating pad. The mice were then treated with a bilateral stereotaxic injection of the virus into the dmPFC (anteroposterior (AP), +1.7 mm; mediolateral (ML), ±0.4 mm; and dorsoventral (DV), −2.3 mm relative to bregma). The virus was infused bilaterally through a microinjector with a 33 G needle. The virus mixture (150 nl) was infused for 10 min. After infusion, the needle was retained at the injection site for an additional 10 minutes before being withdrawn slowly. The mice were allowed to recover for 3 weeks to allow stable transgene expression.

The shRNA target sequences used in the study are listed in Supplementary Table 1. CMV-PTN-shRNA was constructed to knock down the expression of PTN, and CMV-PTPRZ1-shRNA was constructed to knock down the expression of PTPRZ1. AAV-DIO-PTN-shRNA was used to specifically knock down the expression of astrocytic PTN in the dmPFC in Aldh1l1-Cre/ERT2 mice, with the assistance of intraperitoneally administered tamoxifen (Sigma–Aldrich, dissolved in corn oil, 75 mg/kg/day for 5 consecutive days) to ensure the activation of Cre recombinase. CaMKIIα-Cre along with AAV-DIO-PTPRZ1-shRNA was applied to specifically knock down the expression of PTPRZ1 in dmPFC excitatory neurons. We constructed a DIO-PTN-Overexpression (DIO-PTN OE) to overexpress the astrocytic PTN in the dmPFC in Aldh1l1-Cre/ERT2 mice. All Aldh1l1-Cre/ERT2 mice received a 10-day rest for recovery after the consecutive administration of tamoxifen.

For sparse labeling of CaMKIIα+ excitatory neurons in the dmPFC, the mice were bilaterally injected with a total of 400 nL of viral cocktail (1:1) of rAAV-CaMKIIα-FLP-WPRE-pA and rAAV-nEf1α-FDIO-EYFP-WPRE-pA.

Exogenous chemicals administration

For infusions into the dmPFC, mice received 1 μl of 5 μg/ml PTN (MedChemExpress). For microinjections of AKT activator SC79 or AKT inhibitor MK2206, 1 μl of 1 mg/ml SC79 (MedChemExpress; dissolved in dimethyl sulfoxide in saline) or 1 μl of 1 mg/ml MK2206 (MedChemExpress; dissolved in dimethyl sulfoxide in saline) was administered.

Behavioral tests

Open field test (OFT). The mice were placed in an open chamber (50 × 50 × 40 cm), which was made of gray polyvinyl chloride. The mice were allowed to freely explore the apparatus. The mice were gently placed in the center, and movement was recorded for 5 min. The total distance traveled and time spent in the center (25 × 25 cm) were recorded by a video tracking system and analyzed with software (Shanghai Jiliang Software Technology, Co., Ltd.)

Elevated plus maze (EPM). The apparatus consisted of two opposing open arms (35 × 5 cm) and two opposing enclosed arms (35 × 5 × 15 cm), which were connected by a central platform (5 × 5 cm) and positioned 50 cm above the ground. The activity of the experimental subject within the apparatus was tracked for 5 min via an overhead digital video camera. The time spent in the open arms was recorded and analyzed.

Forced swimming test (FST). The FST was performed in a glass cylinder (height 30 cm, diameter 12 cm), which was filled to 25 cm with water (22–24 °C). The mice were placed in the cylinder for 6 min. The first 2 min were for the mice to acclimate, and the duration of immobility was recorded during the last 4 min. The immobility time was recorded and analyzed with software (Shanghai Jiliang Software Technology, Co., Ltd.).

Tail-suspension test (TST). The mice were suspended by the tail 50 cm above the floor. The activity was automatically monitored during the last 4 minutes of the 6-min test with a threshold defining immobility behavior. The latency to the first immobilization was also recorded.

Sucrose preference test (SPT). The mice were acclimated to two bottles (50-ml tubes with fitted ball-point sipper tubes) for 24 h. One bottle was filled with 1% sucrose, and the other was filled with drinking water. Every 12 h, the bottle positions were swapped to prevent position bias. After another 24 h, the amounts of sucrose and water consumed were recorded, and sucrose preference (%) was calculated as sucrose consumption/(sucrose + water consumption) × 100%.

RT-PCR

TRIzol was used to extract total RNA, and reverse transcription was performed following the protocol of the polymerase chain reaction (PCR) production kit (Accurate Biology, AG 11706). The primer sequences of the investigated mRNAs for the PCR assay are shown in

Supplementary Table 2. The reaction cycle conditions were as follows: initial denaturation at 95 °C for 3 min, followed by 40 cycles of 10 s at 95 °C, 20 s at 58 °C, and 10 s at 72 °C. The ratio of mRNA expression in the dmPFC tissues was analyzed via the $2^{-\Delta\Delta CT}$ method.

Western blotting (WB) analysis

Mouse brain tissues were lysed in ice-cold lysis buffer (RIPA buffer with proteinase inhibitor) for 30 min and centrifuged at 10,000 × *g* for 20 min at 4 °C. Protein samples were separated by SDS–PAGE and transferred onto polyvinylidene difluoride (PVDF) membranes (Millipore). The membranes were blocked with 5% milk in TBST for 1 h at room temperature and then incubated with primary antibodies against S100β (1:1000, Proteintech, Cat# 66616), SOX9 (1:1000, Proteintech, Cat# 55152), GFAP (1:1000, Proteintech, Cat# 60190), PTN (1:1000, Proteintech, Cat# 27117), PTPRZ1 (1:1000, Proteintech, Cat# 55125), PSD95 (1:1000, Affinity, Cat# AF5283-50), AKT (1:1000, CST, Cat# 4685), p-AKT (Ser473) (1:1000, CST, Cat# 4060) and GAPDH (1:1000, Fdbio Science, Cat# FD0063) overnight at 4 °C. Information on the antibodies used in the study can be found in Supplementary Table 3. On the next day, the membranes were washed with TBST three times and incubated with horseradish peroxidase (HRP)-conjugated secondary antibodies (Fdbio Science) for 1 h at room temperature. Protein abundance was quantified by analyzing the western blot bands using ImageJ software. Quantified band intensities were normalized to GAPDH levels. Unprocessed scans of the blots are provided in the Source Data file.

Immunohistochemistry (IHC)

The mice were anesthetized with phenobarbital and perfused with 4% PFA in 0.1 M PBS. The brain tissues were postfixed overnight in 4% PFA at 4 °C and transferred to 30% sucrose in 0.1 M PBS. The brain tissues were cut into 20 μm-thick sections on a freezing microtome. Then, the sections were washed with PBS three times and incubated first in a blocking buffer containing 3% bovine serum albumin in 0.2% Triton X-100/PBS for 2 h at room temperature and then with primary antibodies against PTN (1:200, Proteintech, Cat# 27117), PTPRZ1 (1:100, Proteintech, Cat# 55125), S100β (1:200, Proteintech, Cat# 66616), SOX9 (1:200, Invitrogen, Cat# 14-9765-80), and GFAP (1:200, Proteintech, Cat# 60190), in blocking buffer overnight at 4 °C. After that, the sections were incubated with secondary antibody (Cy3 and Alexa fluor 488) at 37 °C for 60 min. The stained sections were examined using with a Nikon confocal microscope equipped, and images were captured with a Nikon DS-Qi2 camera.

Isolation of astrocytes and neurons from the mouse brain

Astrocytes and neurons were isolated from the dmPFC of mice using magnetic-activated cell sorting (MACS)[23]. In brief, after the mice were anesthetized with pentobarbital sodium and perfused with ice-cold sterile PBS, the dmPFC tissue was dissociated at 37 °C for 15 min using the Adult Brain Dissociation Kit (Miltenyi Biotec, Cat# 130-107-677) with a gentleMACS Dissociator (Miltenyi Biotec, Cat# 130-093-235).

To isolate astrocytes, the cells were incubated with FcR Blocking Reagent after the cell pellet was passed through 70-μm nylon mesh. Next, the cells were incubated with Anti-ACSA-2 MicroBeads (Miltenyi Biotec, Cat# 130-097-679) and then subjected to MACS through the LS column.

To isolate neurons, after the brain tissue was dissociated, the cell pellet was treated with cold debris removal solution and red blood cell removal solution. Following the instructions of the Adult Neuron Isolation Kit (Miltenyi Biotec, Cat# 130-126-603), the cells were incubated with the Adult Non-Neuronal Cell Biotin-Antibody Cocktail and Anti-Biotin MicroBeads and then subjected to MACS through the LS column. The specificity of the Anti-ACSA-2 MicroBeads kit and Adult Neuron Isolation Kit was validated and is shown in Supplementary Fig. 9E, F.

Electrophysiological recording

The mice were anesthetized with isoflurane, and the whole brain was quickly dissociated into prechilled and oxygenated dissection fluid containing (in mM) 213 sucrose, 10 glucose, 26 $NaHCO_3$, 3 KCl, 1 $NaH_2PO_4{\cdot}2H_2O$, 10 $MgCl_2$, and 0.5 $CaCl_2$. Acute brain slices (300 μm) containing the dmPFC were acquired in chilled dissection fluid using a microtome (VT1000S, Leica). The sections were transferred to the incubation chamber and immersed in artificial cerebrospinal fluid (in mM; 125 NaCl, 26 $NaHCO_3$, 5 KCl, 1.2 NaH_2PO_4, 2.6 $CaCl_2$, 1.3 $MgCl_2$, and 10 glucose) at 30 °C for 1 h. After incubation, the sections were placed in the slice chamber for electrophysiological recording with continuous perfusion of artificial cerebrospinal fluid (saturated with 95% O_2/5% CO_2).

The dmPFC excitatory neurons were identified by CaMKIIα-EGFP and visualized for recording using an infrared-differential interference contrast microscope (Olympus, Japan). We used patch pipettes (4–8 MΩ, WPI, USA) for the whole-cell patch clamp recordings. The signal was amplified by a MultiClamp 700B amplifier (Molecular Devices, USA). The miniature excitability postsynaptic current (mEPSC) was sampled in the presence of tetrodotoxin (1 μM) and picrotoxin (100 μM) at −70 mV. The patch pipettes were filled with an intracellular solution containing (in mM) 122 potassium-gluconate, 5 NaCl, 2 $MgCl_2$, 0.3 $CaCl_2$, 10 HEPES, 5 EGTA, 4 Mg-ATP, and 0.3 Na_3-GTP. The action potentials were recorded using the injected current (from 0 pA to 120 pA in 20 pA increments, 500 ms duration) without any synaptic transmission blockers. We calculated the number of action potentials induced by each injected current (shown as firing rate–injected current (f–I) curves), frequency (f–I), and amplitude of the mEPSCs using pCLAMP10.7.

Dendritic spine analysis

The mice were bilaterally injected with a total of 400 nL of a viral cocktail (1:1) of rAAV-CaMKIIα-FLP-WPRE-PA or rAAV-nEf1α-FDIO-EYFP-WPRE-PA to label CaMKIIα+ excitatory neurons in the dmPFC. We used laser confocal photography to photograph dendritic spines, acquired multilayer *Z* axes, and reconstructed the dendritic spine image. The spines were classified into one of four morphological subtypes: filopodial, thin, stub, or mushroom-shaped. ImageJ was used (http://rsbweb.nih.gov/ij) to calculate the density of thin, stub, and mushroom-shaped dendritic spines. Approximately ten randomly selected neurons were analyzed per condition across two coverslips. The density of spines was scored in dendritic segments 10 μm in length. Finally, we counted and used the number of dendritic spines per 10 μm to describe the density of the dendritic spines.

Statistical analysis

The statistical methods used for bioinformatics analysis in this paper are indicated in the legend of each figure. For experimental validation, SPSS 21.0 (IBM) was used to analyze the data, which are presented as the means ± SEMs. The normality of the data was examined via the Shapiro–Wilk test. The normally distributed data were tested by a two-sided unpaired *t* test, one- or two-way analysis of variance (ANOVA). The nonnormally distributed data were analyzed by the Wilcoxon test. Statistical significance was set at $^{*}P < 0.05$, $^{**}P < 0.01$, $^{***}P < 0.001$, N.S. not significant.

Reporting summary

Further information on research design is available in the Nature Portfolio Reporting Summary linked to this article.

Data availability

The single-nucleus RNA sequencing data were obtained from the GEO database under the accession number GSE144136. The GWAS summary statistics were obtained from the IEU OpenGWAS database with a GWAS ID of ieu-b-102 (https://gwas.mrcieu.ac.uk/datasets/ieu-b-102/).

These are both public data. There are no restrictions on data availability in the manuscript. The data generated in this study are provided in the Source Data file. Source data are provided with this paper.

Code availability

The codes used for all processing and analysis are available at https://github.com/corrschi/snRNA-seq-of-MDD.

References

1. Marx, W. et al. Major depressive disorder. *Nat. Rev. Dis. Primers* **9**, 44 (2023).
2. Marwaha, S. et al. Novel and emerging treatments for major depression. *Lancet* **401**, 141–153 (2023).
3. Herrman, H. et al. Time for united action on depression: a Lancet–World Psychiatric Association Commission. *Lancet* **399**, 957–1022 (2022).
4. Su, Y. A., Ye, C., Xin, Q. & Si, T. Major depressive disorder with suicidal ideation or behavior in Chinese population: a scoping review of current evidence on disease assessment, burden, treatment and risk factors. *J. Affect. Disord.* **340**, 732–742 (2023).
5. Fox, M. E. & Lobo, M. K. The molecular and cellular mechanisms of depression: a focus on reward circuitry. *Mol. Psychiatry* **24**, 1798–1815 (2019).
6. Erdmann, T. et al. Amygdala reactivity, antidepressant discontinuation, and relapse. *JAMA Psychiatry* **81**, 1081–1089 (2024).
7. Schmaal, L. et al. Cortical abnormalities in adults and adolescents with major depression based on brain scans from 20 cohorts worldwide in the ENIGMA Major Depressive Disorder Working Group. *Mol. Psychiatry* **22**, 900–909 (2016).
8. Sun, S. et al. Resting-state dynamic functional connectivity in major depressive disorder: a systematic review. *Prog. Neuro-Psychopharmacol. Biol. Psychiatry* **135**, 111076 (2024).
9. Dóra, F., Renner, É., Keller, D., Palkovits, M. & Dobolyi, Á. Transcriptome profiling of the dorsomedial prefrontal cortex in suicide victims. *Int. J. Mol. Sci.* **23**, 7067 (2022).
10. Zhang, Z.-Q. et al. Increased prefrontal cortex connectivity associated with depression vulnerability and relapse. *J. Affect. Disord.* **304**, 133–141 (2022).
11. Moriguchi, S. et al. Monoamine oxidase B total distribution volume in the prefrontal cortex of major depressive disorder. *JAMA Psychiatry* **76**, 634–641 (2019).
12. Zhang, T. et al. Altered neural activity in the reward-related circuit and executive control network associated with amelioration of anhedonia in major depressive disorder by electroconvulsive therapy. *Prog. Neuro-Psychopharmacol. Biol. Psychiatry* **109**, 110193 (2021).
13. Pan, Y. et al. Prefrontal cortex astrocytes in major depressive disorder: exploring pathogenic mechanisms and potential therapeutic targets. *J. Mol. Med.* **102**, 1355–1369 (2024).
14. Li, D. et al. Neurophysiological markers of disease severity and cognitive dysfunction in major depressive disorder: a TMS-EEG study. *Int. J. Clin. Health Psychol.* **24**, 100495 (2024).
15. Woodham, R. D. et al. Home-based transcranial direct current stimulation treatment for major depressive disorder: a fully remote phase 2 randomized sham-controlled trial. *Nat. Med.* **31**, 87–95 (2025).
16. Scho, S., Brüchle, W., Schneefeld, J. & Rosenkranz, K. Enhancing neuroplasticity in major depression: a novel 10 Hz-rTMS protocol is more effective than iTBS. *J. Affect. Disord.* **367**, 109–117 (2024).
17. Huang, J. et al. A neuronal circuit for activating descending modulation of neuropathic pain. *Nat. Neurosci.* **22**, 1659–1668 (2019).
18. Seamans, J. K., Lapish, C. C. & Durstewitz, D. Comparing the prefrontal cortex of rats and primates: insights from electrophysiology. *Neurotox. Res.* **14**, 249–262 (2008).
19. Banasr, M. et al. Glial pathology in an animal model of depression: reversal of stress-induced cellular, metabolic and behavioral deficits by the glutamate-modulating drug riluzole. *Mol. Psychiatry* **15**, 501–511 (2008).
20. Codeluppi, S. A. et al. Chronic stress alters astrocyte morphology in mouse prefrontal cortex. *Int. J. Neuropsychopharmacol.* **24**, 842–853 (2021).
21. Riga, M. S. et al. Scn1a haploinsufficiency in the prefrontal cortex leads to cognitive impairment and depressive phenotype. *Brain* **147**, 4169–4184 (2024).
22. Paton, S. E. J. & Menard, C. Glutamate shall not pass: a mechanistic role for astrocytic O-GlcNAc transferase in stress and depression. *J. Clin. Investig.* **133**, e168662 (2023).
23. Guo, F. et al. Astrocytic ALKBH5 in stress response contributes to depressive-like behaviors in mice. *Nat. Commun.* **15**, 4347 (2024).
24. Wang, Q., Jie, W., Liu, J. H., Yang, J. M. & Gao, T. M. An astroglial basis of major depressive disorder? An overview. *Glia* **65**, 1227–1250 (2017).
25. Lu, C.-L., Ren, J. & Cao, X. An astroglial basis of major depressive disorder: molecular, cellular, and circuit features. *Biol. Psychiatry* **97**, 217–226 (2025).
26. Liu, J. et al. Astrocyte dysfunction drives abnormal resting-state functional connectivity in depression. *Sci. Adv.* **8**, eabo2098 (2022).
27. Mo, J. W. et al. Lysosomal TFEB-TRPML1 axis in astrocytes modulates depressive-like behaviors. *Adv. Sci.* **11**, 2403389 (2024).
28. Torres-Platas, S. G. et al. Astrocytic hypertrophy in anterior cingulate white matter of depressed suicides. *Neuropsychopharmacology* **36**, 2650–2658 (2011).
29. Lin, S.-S. et al. Electroacupuncture prevents astrocyte atrophy to alleviate depression. *Cell Death Dis.* **14**, 343 (2023).
30. Rajkowska, G. & Stockmeier, C. Astrocyte pathology in major depressive disorder: insights from human postmortem brain tissue. *Curr. Drug Targets* **14**, 1225–1236 (2013).
31. Rajkowska, G. et al. Morphometric evidence for neuronal and glial prefrontal cell pathology in major depression. *Biol. Psychiatry* **45**, 1085–1098 (1999).
32. Banasr, M. & Duman, R. S. Glial loss in the prefrontal cortex is sufficient to induce depressive-like behaviors. *Biol. Psychiatry* **64**, 863–870 (2008).
33. Fang, Y. et al. Fluoxetine inhibited the activation of A1 reactive astrocyte in a mouse model of major depressive disorder through astrocytic 5-HT2BR/β-arrestin2 pathway. *J. Neuroinflammation* **19**, 23 (2022).
34. Codeluppi, S. A. et al. Prefrontal cortex astroglia modulate anhedonia-like behavior. *Mol. Psychiatry* **28**, 4632–4641 (2023).
35. Lei, L., Wang, Y.-F., Chen, C.-Y., Wang, Y.-T. & Zhang, Y. Novel insight into astrocyte-mediated gliotransmission modulates the synaptic plasticity in major depressive disorder. *Life Sci.* **355**, 122988 (2024).
36. Tao, C. et al. Excitation-inhibition imbalance in medial preoptic area circuits underlies chronic stress-induced depression-like states. *Nat. Commun.* **15**, 8575 (2024).
37. Tang, C. et al. Neural stem cells behave as a functional niche for the maturation of newborn neurons through the secretion of PTN. *Neuron* **101**, 32–44.e6 (2019).
38. Nikolakopoulou, A. M. et al. Pericyte loss leads to circulatory failure and pleiotrophin depletion causing neuron loss. *Nat. Neurosci.* **22**, 1089–1098 (2019).
39. Stefanov, A. et al. Depression-like behavior is associated with deficits in cognition and hippocampal neurogenesis in a subset of spinally contused male, but not female, rats. *Brain Behav. Immun.* **123**, 270–287 (2025).
40. Rodríguez-Zapata, M. et al. Pleiotrophin modulates acute and long-term LPS-induced neuroinflammatory responses and hippocampal neurogenesis. *Toxicology* **509**, 153947 (2024).

41. Galán-Llario, M. et al. Pleiotrophin overexpression reduces adolescent ethanol consumption and modulates ethanol-induced glial responses and changes in the perineuronal nets in the mouse hippocampus. *CNS Neurosci. Ther.* **30**, e70159 (2024).
42. Qiu, X. et al. Single-cellRNA-sequencing analysis reveals enhanced non-canonical neurotrophic factor signaling in the subacute phase of traumatic brain injury. *CNS Neurosci. Ther.* **29**, 3446–3459 (2023).
43. Linnerbauer, M. et al. Astrocyte-derived pleiotrophin mitigates late-stage autoimmune CNS inflammation. *Front. Immunol.* **12**, 800128 (2022).
44. Li, H. et al. Pleiotrophin ameliorates age-induced adult hippocampal neurogenesis decline and cognitive dysfunction. *Cell Rep.* **42**, 113022 (2023).
45. Zhou, Y. et al. The combination of quantitative proteomics and systems genetics analysis reveals that PTN is associated with sleep-loss-induced cognitive impairment. *J. Proteome Res.* **22**, 2936–2949 (2023).
46. Asai, H., Yokoyama, S., Morita, S., Maeda, N. & Miyata, S. Functional difference of receptor-type protein tyrosine phosphatase ζ/β isoforms in neurogenesis of hippocampal neurons. *Neuroscience* **164**, 1020–1030 (2009).
47. Pavlov, I., Rauvala, H. & Taira, T. Enhanced hippocampal GABAergic inhibition in mice overexpressing heparin-binding growth-associated molecule. *Neuroscience* **139**, 505–511 (2006).
48. Nagy, C. et al. Single-nucleus transcriptomics of the prefrontal cortex in major depressive disorder implicates oligodendrocyte precursor cells and excitatory neurons. *Nat. Neurosci.* **23**, 771–781 (2020).
49. Cui, L. et al. Major depressive disorder: hypothesis, mechanism, prevention and treatment. *Signal Transduct. Target Ther.* **9**, 30 (2024).
50. Torres-Platas, S. G., Nagy, C., Wakid, M., Turecki, G. & Mechawar, N. Glial fibrillary acidic protein is differentially expressed across cortical and subcortical regions in healthy brains and downregulated in the thalamus and caudate nucleus of depressed suicides. *Mol. Psychiatry* **21**, 509–515 (2016).
51. Du Preez, A. et al. Chronic stress followed by social isolation promotes depressive-like behaviour, alters microglial and astrocyte biology and reduces hippocampal neurogenesis in male mice. *Brain Behav. Immun.* **91**, 24–47 (2021).
52. Schmitz, F. et al. Methylphenidate decreases ATP levels and impairs glutamate uptake and Na(+),K(+)-ATPase activity in juvenile rat hippocampus. *Mol. Neurobiol.* **54**, 7796–7807 (2017).
53. Petrik, D., Lagace, D. C. & Eisch, A. J. The neurogenesis hypothesis of affective and anxiety disorders: are we mistaking the scaffolding for the building? *Neuropharmacology* **62**, 21–34 (2012).
54. Cui, W. et al. Glial dysfunction in the mouse habenula causes depressive-like behaviors and sleep disturbance. *J. Neurosci.* **34**, 16273–16285 (2014).
55. Rauvala, H. et al. Heparin-binding proteins HB-GAM (pleiotrophin) and amphoterin in the regulation of cell motility. *Matrix Biol.* **19**, 377–387 (2000).
56. Lauri, S. E., Rauvala, H., Kaila, K. & Taira, T. Effect of heparin-binding growth-associated molecule (HB-GAM) on synaptic transmission and early LTP in rat hippocampal slices. *Eur. J. Neurosci.* **10**, 188–194 (2009).
57. Herradón, G. & Pérez-García, C. Targeting midkine and pleiotrophin signalling pathways in addiction and neurodegenerative disorders: recent progress and perspectives. *Br. J. Pharmacol.* **171**, 837–848 (2014).
58. Seo, J. S. et al. Cellular and molecular basis for stress-induced depression. *Mol. Psychiatry* **22**, 1440–1447 (2016).
59. Thompson, S. M. et al. An excitatory synapse hypothesis of depression. *Trends Neurosci.* **38**, 279–294 (2015).
60. Li, Z., Ruan, M., Chen, J. & Fang, Y. Major depressive disorder: advances in neuroscience research and translational applications. *Neurosci. Bull.* **37**, 863–880 (2021).
61. Lener, M. S. et al. Glutamate and gamma-aminobutyric acid systems in the pathophysiology of major depression and antidepressant response to ketamine. *Biol. Psychiatry* **81**, 886–897 (2017).
62. Zhuang, L. et al. LHPP in glutamatergic neurons of the ventral hippocampus mediates depression-like behavior by dephosphorylating CaMKIIα and ERK. *Biol. Psychiatry* **95**, 389–402 (2024).
63. Nedergaard, M., Ransom, B. & Goldman, S. A. New roles for astrocytes: redefining the functional architecture of the brain. *Trends Neurosci.* **26**, 523–530 (2003).
64. Choleva, E. et al. Targeting the interaction of pleiotrophin and VEGFA(165) with protein tyrosine phosphatase receptor zeta 1 inhibits endothelial cell activation and angiogenesis. *Eur. J. Pharm.* **977**, 176692 (2024).
65. Nagai, K., Fujii, M. & Kitazume, S. Protein tyrosine phosphatase receptor type Z in central nervous system disease. *Int. J. Mol. Sci.* **23**, 4414 (2022).
66. Tanga, N. et al. The PTN-PTPRZ signal activates the AFAP1L2-dependent PI3K-AKT pathway for oligodendrocyte differentiation: targeted inactivation of PTPRZ activity in mice. *Glia* **67**, 967–984 (2019).
67. Qin, H. et al. Antidepressant effects of esketamine via the BDNF/AKT/mTOR pathway in mice with postpartum depression and their offspring. *Prog. Neuro-Psychopharmacol. Biol. Psychiatry* **132**, 110992 (2024).
68. Zhu, Y.-J. et al. Autophagy dysfunction contributes to NLRP1 inflammasome-linked depressive-like behaviors in mice. *J. Neuroinflammation* **21**, 6 (2024).
69. Wu, Y. et al. Levomilnacipran improves lipopolysaccharide-induced dysregulation of synaptic plasticity and depression-like behaviors via activating BDNF/TrkB mediated PI3K/Akt/mTOR signaling pathway. *Mol. Neurobiol.* **61**, 4102–4115 (2023).
70. Labonté, B. et al. Sex-specific transcriptional signatures in human depression. *Nat. Med.* **23**, 1102–1111 (2017).
71. Martin, L. A., Neighbors, H. W. & Griffith, D. M. The experience of symptoms of depression in men vs women. *JAMA Psychiatry* **70**, 1100–1106 (2013).
72. Seney, M. L. et al. Opposite molecular signatures of depression in men and women. *Biol. Psychiatry* **84**, 18–27 (2018).
73. Li, X. et al. The effects of tamoxifen on mouse behavior. *Genes Brain Behav.* **19**, e12620 (2020).
74. Mathys, H. et al. Single-cell transcriptomic analysis of Alzheimer's disease. *Nature* **570**, 332–337 (2019).
75. Jakel, S. et al. Altered human oligodendrocyte heterogeneity in multiple sclerosis. *Nature* **566**, 543–547 (2019).
76. Guo, X. et al. Global characterization of T cells in non-small-cell lung cancer by single-cell sequencing. *Nat. Med.* **24**, 978–985 (2018).
77. Zhang, L. et al. Lineage tracking reveals dynamic relationships of T cells in colorectal cancer. *Nature* **564**, 268–272 (2018).
78. Jin, S. et al. Inference and analysis of cell-cell communication using CellChat. *Nat. Commun.* **12**, 1088 (2021).
79. Browaeys, R., Saelens, W. & Saeys, Y. NicheNet: modeling intercellular communication by linking ligands to target genes. *Nat. Methods* **17**, 159–162 (2019).
80. Zhou, Y. et al. Metascape provides a biologist-oriented resource for the analysis of systems-level datasets. *Nat. Commun.* **10**, 1523 (2019).
81. Liberzon, A. et al. The molecular signatures database hallmark gene set collection. *Cell Syst.* **1**, 417–425 (2015).
82. Ma, Y. et al. Polygenic regression uncovers trait-relevant cellular contexts through pathway activation transformation of single-cell RNA sequencing data. *Cell Genomics* **3**, 100383 (2023).
83. Zhu, X. et al. Distinct thalamocortical circuits underlie allodynia induced by tissue injury and by depression-like states. *Nat. Neurosci.* **24**, 542–553 (2021).

84. Cathomas, F. et al. Circulating myeloid-derived MMP8 in stress susceptibility and depression. *Nature* **626**, 1108–1115 (2024).

Acknowledgements

This work was supported by the National Natural Science Foundation of China (82071237 to OUYHD, 82401437 to B.X.H.) and the Guangdong Basic and Applied Basic Research Foundation (2023A1515010147 to OUYHD, 2023A1515011180 to B.X.H.).

Author contributions

All authors read and approved the final manuscript. O.U.Y.H.D. and C.D.M. designed the experiments. Z.K., Z.J.X., H.Z.L., H.W., and Z.H.X. performed the experiments and collected the data. C.D.M., Z.K., Z.J.X., L.Y., H.J.X., and O.C.P. performed the analysis. O.C.P., C.D.M., B.X.H., Z.W.A., and O.U.Y.H.D. wrote the manuscript. O.U.Y.H.D. and O.C.P. supervised this study. All the authors reviewed the manuscript.

Competing interests

The authors declare no competing interests.

Additional information

Supplementary information The online version contains supplementary material available at https://doi.org/10.1038/s41467-025-57924-1.

Correspondence and requests for materials should be addressed to Xiaohui Bai, Chaopeng Ou or Handong Ouyang.

Peer review information *Nature Communications* thanks Xiong Cao and the other anonymous reviewer(s) for their contribution to the peer review of this work. A peer review file is available.